Supporting Information

Diarylboryl–Phenoselenazine Hybrid AIEgens: Design, Synthesis, and Multimodal Stimuli-Responsive Properties

Yan Wang,[a] Zengheng Wen,[a] Zhuang Luo,[a] Runze Han,[a] Xingliang Liu [a]* and Weidong Zhang [a]*

[a]School of Chemical Engineering, Qinghai University, Xining, 810016, China;
Correspondence: Weidong Zhang (13772405930@163.com)

Contents

1. Materials and instrumentation

General. All reactions were performed using standard Schlenk and glovebox (Vigor) techniques of SG1200/750TS-F system under argon atmosphere. Tetrahydrofuran and toluene were distilled from sodium/benzophenone prior to use. *n*-butyllithium (2.5 M, in hexane), fluorodimesitylborane (98%), bis(dibenzylideneacetone) palladium (Pd_2dba_3) (99%), and tetrakis(triphenylphosphine) palladium ($Pd(Ph_3P)_4$) (99%) were purchased from Energy Chemical Inc. Phenoselenazine and trimethyl(phenyl) stannane were prepared according to literature procedures[1,2]. Unless otherwise indicated, all other reagents and solvents were used as commercially available without further purification.

NMR spectra were measured on a Bruker Avance-600 spectrometer in the solvents indicated; chemical shifts are reported in units (ppm) by assigning TMS resonance in the ^1H spectrum as 7.26 ppm, $CDCl_3$ resonance in the ^{13}C spectrum as 77.0 ppm. Coupling constants are reported in Hz with multiplicities denoted as s (singlet), d (doublet), t (triplet), q (quartet) and m (multiplet). UV-vis measurements were performed using DH-2000-BAL Scan spectrophotometer. Fluorescence measurements were conducted on an FLS920 system and MicroTEQ-R1 system of ocean optics. Low-temperature environment was carried through Unistat905w model of equipment. Depressurization and remove the solvent were achieved using RV10 system of IKA. Single crystal X-ray diffraction analysis was carried out on a XtaLABSynergy-Dw instrument. The cyclic voltammetry (CV) was measured using a Metrohm PGSTAT204 set up.

2. Experimental procedures and data

2.1 Synthesis of 10-(dimesitylboraneyl)-10H-phenoselenazine (4a):

To a solution of phenoselenazine (1.23 g, 5.00 mmol) in THF (30 mL) at -78 °C was added dropwise a solution of *n*-BuLi (2.5 M in hexanes, 2.4 mL, 6.0 mmol) via syringe. After the reaction mixture was stirred for another 30 min at -78 °C, A solution of Mes_2BF

(1.41 g, 5.27 mmol) in THF was then added dropwise at -78 °C, and the mixture was warmed to room temperature and stirred overnight. The solvent was removed under reduced pressure from the cloudy mixture and the product was extracted with 60 mL DCM, and the mixture was filtered through Celite. The solvent was removed from the filtrate，the crude product was subjected to purification by column chromatography (silica gel; petroleum ether/DCM, v/ v = 20/1), affording a white solid. Yield: 2.25 g (**91**%). ^{1}H NMR (600 MHz, $CDCl_3$): δ 7.40 (dd, 2H, *J* = 11.4 Hz, J = 1.8 Hz, Ar*H*), 7.27 (d, 2H, *J* = 10.2 Hz, Ar*H*), 6.98-6.89 (m, 4H, Ar*H*), 6.65 (s, 4H, Ar*H*), 2.41 (s, 12H, CH_3), 2.18 (s, 6H, CH_3); ^{13}C NMR (101 MHz, $CDCl_3$): δ 143.79, 140.44, 136.83, 129.77, 128.00, 126.65, 126.50, 125.45, 24.82, 20.91. HRMS (APCI) *m/z*: [M] calcd for $C_{30}H_{30}BNSe$, 495.1636, found, 495.1634. Anal. Calcd. For $C_{30}H_{30}BNSe$: C, 72.89; H, 6.12; N, 2.83. Found: C, 72.81; H, 6.08; N, 2.79.

2.2 Synthesis of 10-(4-(dimesitylboraneyl)phenyl)-10H-phenoselenazine (4b):

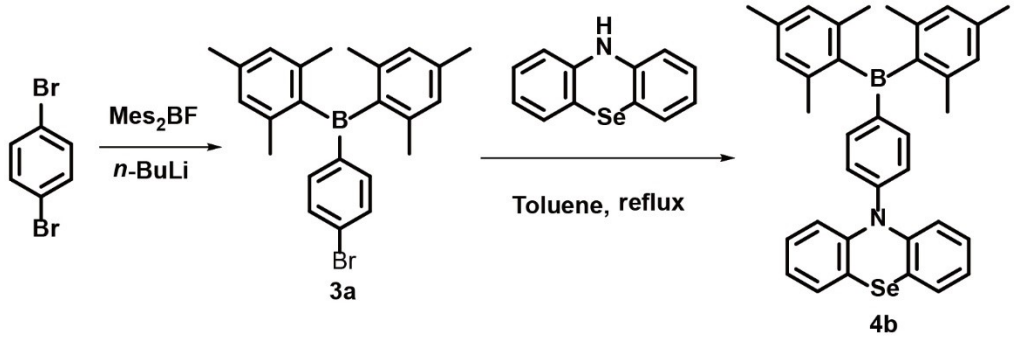

A solution of *para*-dibromobenzene (0.440 g, 1.864 mmol, 2 eq.) was prepared in anhydrous THF (10 mL) and cooled to -78 °C. To the cooled solution, 2.5 M *n*BuLi in hexanes (0.78 mL, 1.864 mmol, 2 eq.) was added dropwise over 20 minutes and the

solution was stirred at -78 °C for 1 hour. Dimesitylfluoroborane (0.250 g, 0.932 mmol, 1 eq.) was dissolved in anhydrous THF and transferred to an addition funnel before being added dropwise to the previous solution at -78 °C. The solution was stirred at -78 °C for 1 hour before being allowed to warm to room temperature while stirring overnight. Distilled water (5 mL) was added to quench the reaction and the mixture was extracted with CH_2Cl_2, washed with distilled water, and dried over sodium sulfate. The crude material was filtered before purification by column chromatography using hexanes as eluent. The product A was isolated as a white solid.

Under an inert atmosphere, a 250 mL Schlenk flask was charged with a 90 mL anhydrous toluene solution of **3a** (1.65 g, 4.08 mmol), phenoselenazine (1.01 g, 4.08 mmol), Pd_2dba_3 (0.17 g, 0.12 mmol), tri-*tert*-butylphosphonium tetrafluoroborate (0.06 g, 0.204 mmol), and sodium *tert*-butoxide (0.78 g, 8.16 mmol). The flask was equipped with a reflux condenser and heated to reflux under nitrogen for 24 hours. The reaction was quenched with 10 mL of distilled water and extracted with dichloromethane. The organic layer was dried over sodium sulfate and purified by column chromatography using petroleum ether /DCM (5:1 v/v). The product was isolated as a bright yellow solid (1.61g, 69 % yield). ^{1}H NMR (600 MHz, $CDCl_3$): δ 7.56 (d, 2H, J = 7.2 Hz, Ar*H*), 7.43 (d, 2H, J = 7.8 Hz, Ar*H*), 7.37 (d, 2H, J = 7.8 Hz, Ar*H*), 7.30 (t, 2H, J = 7.2 Hz, Ar*H*), 7.14 (t, 2H, J = 7.2 Hz, Ar*H*), 6.91 (d, 2H, J = 7.8 Hz, Ar*H*), 6.78 (s, 4H Ar*H*), 2.28 (s, 6H, CH_3), 2.03 (s, 12H, CH_3); ^{13}C NMR (151 MHz, $CDCl_3$) δ 148.70, 141.71, 140.69, 139.02, 137.98,

131.22, 130.16, 128.00, 127.49, 127.15, 126.02, 114.97, 23.49, 21.16. HRMS (APCI) *m/z*: $[M + H]^+$ calcd for $C_{36}H_{35}BNSe$, 572.2027 found, 572.2017. Anal. Calcd. For $C_{36}H_{34}BNSe$: C, 75.80; H, 6.01; N, 2.46. Found: C, 75.73; H, 5.94; N, 2.43.

2.3 Synthesis of 10-(4'-(dimesitylboraneyl)-[1,1'-biphenyl]-4-yl)-10H-phenoselenazine (4c):

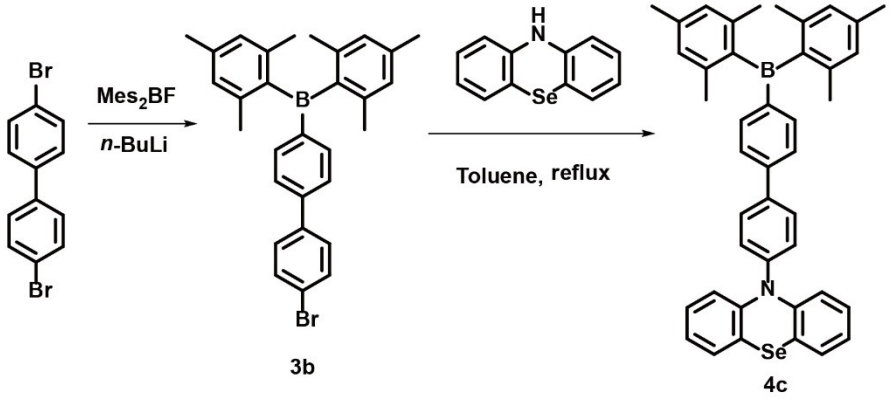

Compound **4c** was prepared following a procedure similar to that used for compound **4b**. The quantities involved and characterization data are as follows: **3b** (1.96 g, 4.08 mmol), **3a** (1.65 g, 4.08 mmol), phenoselenazine (1.01 g, 4.08 mmol), Pd_2dba_3 (0.17 g, 0.12 mmol), tri-*tert*-butylphosphonium tetrafluoroborate (0.06 g, 0.204 mmol), and sodium *tert*-butoxide (0.78 g, 8.16 mmol). The crude product was subjected to purification by column chromatography (silica gel; petroleum ether/DCM, v/v = 5/1), affording a white solid. Yield: 1.9 g (72%).^{1}H NMR (600 MHz, $CDCl_3$): δ 7.72 (d, 2H, J = 7.8 Hz, Ar*H*), 7.60 (s, 4H, Ar*H*), 7.38 (d, 2H, J = 7.8 Hz, Ar*H*), 7.29 (d, 2H, J = 7.8 Hz, Ar*H*), 7.11 (t, 2H, J = 7.8 Hz, Ar*H*), 6.99 (t, 2H, J = 7.2 Hz, Ar*H*), 6.91 (d, 2H, J = 8.4 Hz, Ar*H*), 6.85 (s, 4H Ar*H*), 2.33 (s, 6H, C*H*$_3$), 2.05 (s, 12H, C*H*$_3$); ^{13}C NMR (151 MHz, $CDCl_3$) δ 143.53,

143.47, 140.85, 138.64, 137.22, 137.18, 130.25, 128.67, 128.21, 127.41, 126.23, 124.92, 124.35, 122.47, 121.92, 23.50, 21.25. HRMS (APCI) *m/z*: $[M + H]^+$ calcd for $C_{42}H_{39}BNSe$, 648.2340, found, 648.2334. Anal. Calcd. For $C_{42}H_{38}BNSe$: C, 78.02; H, 5.92; N, 2.17. Found: C, 77.96; H, 5.88; N, 2.08.

2.4 Synthesis of 10-(dimesitylboraneyl)-3,7-diphenyl-10H-phenoselenazine (4d):

Pd_2dba_3（0.19g, 0.21mmol）, tri(o-tolyl)phosphine （0.20g, 0.66mmol）, compound **3** (2.61 g, 4.0 mmol) and trimethyl(phenyl) stannane (2.32 g, 9.6 mmol) were dissolved in 100 mL of toluene in a Schlenk flask. The mixture was refluxed in argon atmosphere for 12 h. After the removal of the solvent at a reduced pressure, the residue was purified by column chromatography on a silica gel column with petroleum ether/dichloromethane (3:1 by volume) to obtain an white solid (1.97 g, 76 %). ^{1}H NMR (600 MHz, $CDCl_3$): δ 7.66 (d, 2H, J = 1.2 Hz, Ar*H*), 7.50 (d, 4H, J = 7.8 Hz, Ar*H*), 7.38 (t, 4H, J = 7.2 Hz, Ar*H*), 7.32 (t, 4H, J = 7.2 Hz, Ar*H*), 7.16 (dd, 2H, J = 9.0 Hz, J = 1.8 Hz, Ar*H*), 6.67 (s, 4H, Ar*H*), 2.45 (s, 12H, CH_3), 2.18 (s, 6H, CH_3); ^{13}C NMR (101 MHz, $CDCl_3$): δ 143.79, 143.09, 140.51, 140.45, 139.57, 138.27, 137.02, 136.84, 129.79, 128.77, 128.18, 128.12, 128.07, 128.02, 127.44, 126.86, 126.74, 126.67, 126.58, 126.51, 125.59, 125.48, 24.77, 20.97, 20.93. HRMS (APCI) *m/z*: [M] calcd for $C_{42}H_{38}BNSe$, 647.2262 found, 647.2251. Anal. Calcd. For $C_{42}H_{38}BNSe$: C, 78.02; H, 5.92; N, 2.17. Found: C, 77.98; H, 5.90; N, 2.14.

2.5 Synthesis of 3,7-di([1,1'-biphenyl]-4-yl)-10-(dimesitylboraneyl)-10H-phenoselenazine (4e):

Compound **4e** was prepared following a procedure similar to that used for compound **4d**. The quantities involved and characterization data are as follows: Pd_2dba_3（0.19g, 0.21mmol）, tri(o-tolyl)phosphine （0.20g, 0.66mmol）, compound **3** (2.61 g, 4.0 mmol) and [1,1'-biphenyl]-4-yltrimethylstannane (3.05 g, 9.6 mmol) in 100 mL of toluene. The crude product was purified by column chromatography on a silica gel column with petroleum ether/dichloromethane (3:1 by volume) to obtain an white solid (2.59 g, 81 %). ^{1}H NMR (600 MHz, $CDCl_3$): δ 7.73 (s, 2H, Ar*H*), 7.61-7.58 (m, 12H, Ar*H*), 7.45 (t, 4H, J = 7.2 Hz, Ar*H*), 7.36 (d, 4H, J = 7.8 Hz, Ar*H*), 7.21 (d, 2H, J = 8.4 Hz, Ar*H*), 6.69 (s, 4H, Ar*H*), 2.47 (s, 12H, CH_3), 2.20 (s, 6H, CH_3); ^{13}C NMR (101 MHz, $CDCl_3$): δ 143.16, 140.61, 140.53, 140.28, 138.42, 137.73, 137.06, 128.86, 128.15, 128.04, 127.49, 127.43, 127.19, 127.05, 126.90, 126.64, 125.38, 24.79, 20.98. HRMS (APCI) *m/z*: [M] calcd for $C_{54}H_{46}BNSe$, 799.2888 found, 799.2900. Anal. Calcd. For $C_{54}H_{46}BNSe$: C, 81.20; H, 5.81; N, 1.75. Found: C, 81.13; H, 5.78; N, 1.71.

3. Single-crystal X-ray structure determination

X-ray Crystallography. All data were collected by a XtaLABSynergy-Dw CCD detector diffractometer using Mo/Cu Kα radiation. The data were corrected for absorption through Gaussian integration from indexing of the crystal faces. Structures were solved using the direct methods programs SHELXS-97, and refinements were completed using the program SHELXL-97.

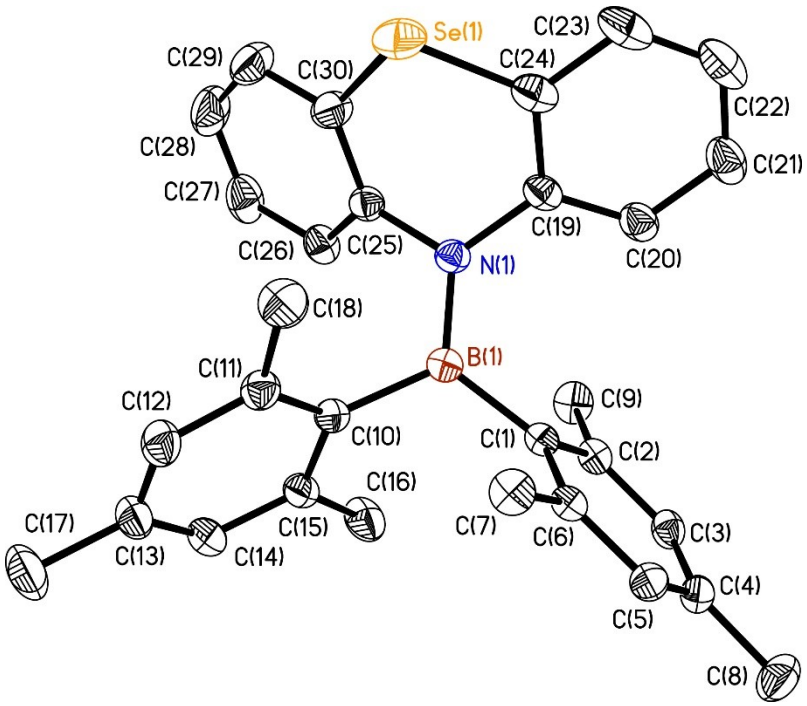

Figure S1. Molecular Structure of **4a** (CCDC 2488433) with thermal ellipsoids presented at a 50% probability level. All hydrogen atoms have been omitted for clarity. Selected bond lengths (Å): Se(1)-C(30), 1.893(2); C(19)-C(24), 1.402(3); Se(1)-C(24), 1.895(2); C(11)-C(12), 1.395(3); N(1)-C(19), 1.449(2); C(11)-C(18), 1.510(3); N(1)-C(25), 1.441(2); C(15)-C(14), 1.391(3); N(1)-B(1), 1.439(2); C(15)-C(16), 1.508(3). Bond angles (deg): C(30)-Se(1)-C(24), 93.81(9); C(14)-C(15)-C(16), 117.28(18); C(25)-N(1)-C(19), 114.85(14); C(26)-C(25)-N(1), 118.83(17); B(1)-N(1)-C(19), 125.97(15); C(30)-C(25)-N(1), 122.48(17); B(1)-N(1)-C(25), 119.18(14); C(30)-C(25)-C(26), 118.66(18), C(1)-B(1)-C(10), 117.78(15).

Table S1. Crystallographic experimental details for compound **4a** (CCDC 2488433).

Identification code	**4a**
Empirical formula	$C_{30}H_{30}BNSe$
Formula weight	494.32
Temperature/K	301.38(10)
Crystal system	monoclinic
Space group	C2/c
a/Å	13.8116(2)
b/Å	19.9217(3)
c/Å	18.5525(3)
α/°	90
β/°	96.064(2)
γ/°	90
Volume/Å3	5076.17(14)
Z	8
$\rho_{calc}g/cm^3$	1.294
μ/mm^{-1}	2.117
F(000)	2048.0
Crystal size/mm^3	0.12 × 0.11 × 0.1
Radiation	Cu Kα (λ = 1.54184)
2Θ range for data collection/°	7.818 to 153.788
Index ranges	$-17 \leq h \leq 13$, $-24 \leq k \leq 22$, $-23 \leq l \leq 23$
Reflections collected	18077
Independent reflections	5091 [R_{int} = 0.0204, R_{sigma} = 0.0181]
Data/restraints/parameters	5091/0/304
Goodness-of-fit on F^2	1.067
Final R indexes [I>=2σ (I)]	R1 = 0.0417, wR2 = 0.1211
Final R indexes [all data]	R1 = 0.0448, wR2 = 0.1242
Largest diff. peak/hole / e $Å^{-3}$	0.59/-0.91

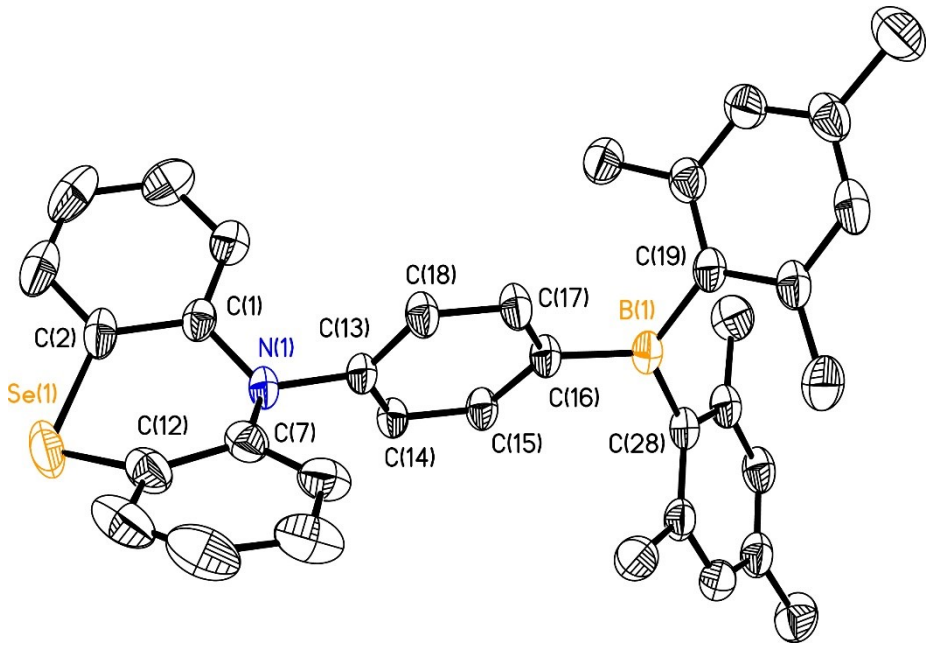

Figure S2. Molecular Structure of **4b** (CCDC 2463488) with thermal ellipsoids presented at a 50% probability level. All hydrogen atoms have been omitted for clarity. Selected bond lengths (Å): Se(1)-C(2), 1.900(5); C(17)-C(18), 1.397(6); Se(1)-C(12), 1.903(6); C(19)-C(20), 1.416(7); N(1)-C(1), 1.420(5); C(19)-C(24), 1.400(7); N(1)-C(7), 1.420(6); C(19)-B(1), 1.579(7); N(1)-C(13), 1.451(4); C(20)-C(21), 1.394(8); C(1)-C(2), 1.403(5); C(20)-C(27), 1.498(8); C(1)-C(6), 1.377(6); C(21)-C(22), 1.358(9). Bond angles (deg): C(2)-Se(1)-C(12), , 95.2(2); C(1)-N(1)-C(13), 116.0(3); C(20)-C(19)-B(1), 120.2(4); C(7)-N(1)-C(1), 122.4(3); C(7)-N(1)-C(13), 116.0(3); C(24)-C(19)-B(1), 121.7(4); C(2)-C(1)-N(1), 121.0(4); C(6)-C(1)-N(1), 121.9(3); C(1)-C(2)-Se(1), 120.1(3); C(22)-C(21)-C(20), 123.4(5); C(3)-C(2)-Se(1), 118.5(4); C(12)-C(7)-N(1), 120.7(4); C(8)-C(7)-N(1), 122.8(5); C(29)-C(28)-B(1), 120.5(4); C(8A)-C(7)-N(1), 121.6(8); C(33)-C(28)-B(1), 121.5(4); C(8A)-C(7)-C(12), 116.5(9); C(7)-C(12)-Se(1), 120.1(4);

Table S2. Crystallographic experimental details for compound **4b** (CCDC 2463488).

Empirical formula	$C_{36}H_{34}BNSe$
Formula weight	570.41
Temperature/K	301.15
Crystal system	monoclinic
Space group	$P2_1$
a/Å	8.9114(2)
b/Å	9.6033(3)
c/Å	17.7481(4)
α/°	90
β/°	103.300(2)
γ/°	90
Volume/Å^3	1478.12(7)
Z	2
ρ_{calc}g/cm^3	1.282
μ/mm^{-1}	1.891
F(000)	592.0
Crystal size/mm^3	0.15 × 0.12 × 0.1
Radiation	Cu Kα (λ = 1.54184)
2Θ range for data collection/°	5.116 to 153.644
Index ranges	$-8 \leq h \leq 11$, $-9 \leq k \leq 11$, $-22 \leq l \leq 21$
Reflections collected	10777
Independent reflections	5018 [R_{int} = 0.0322, R_{sigma} = 0.0396]
Data/restraints/parameters	5018/138/395
Goodness-of-fit on F^2	1.055
Final R indexes [I>=2σ (I)]	R_1 = 0.0452, wR_2 = 0.1207
Final R indexes [all data]	R_1 = 0.0511, wR_2 = 0.1259
Largest diff. peak/hole / e Å^{-3}	0.77/-0.50
Flack parameter	-0.008(13)

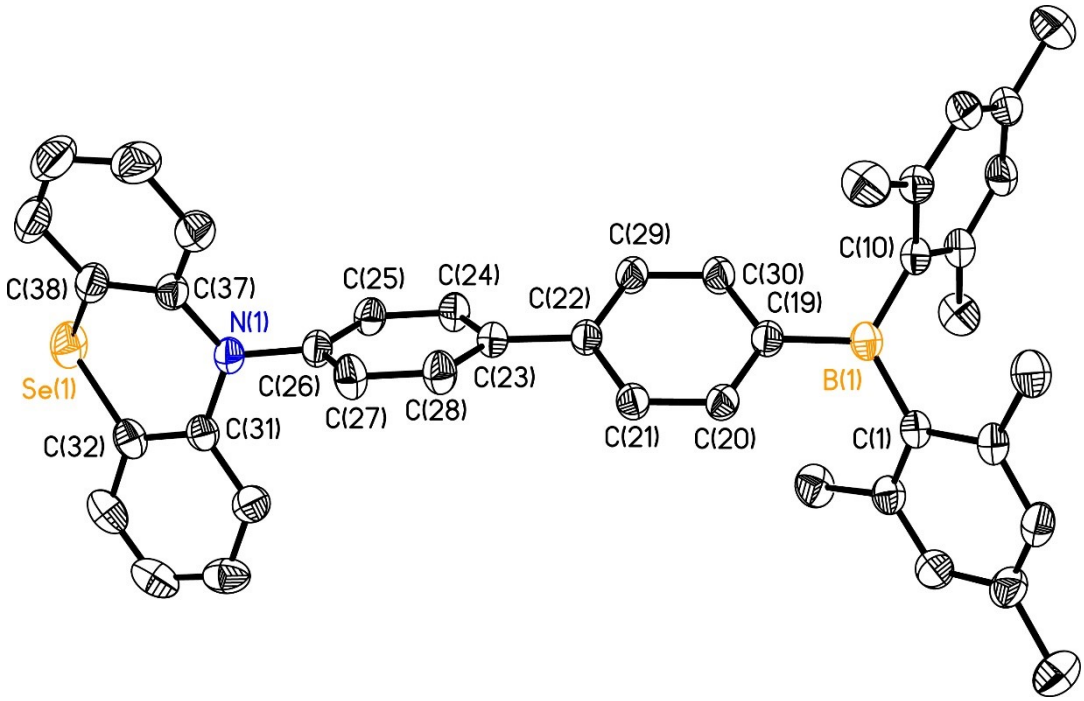

Figure S3. Molecular Structure of 4c (CCDC 2463490) with thermal ellipsoids presented at a 50% probability level. All hydrogen atoms have been omitted for clarity. Selected bond lengths (Å): Se(1)-C(38), 1.899(2); Se(1)-C(32), 1.895(2); N(1)-C(37), 1.413(2); N(1)-C(26), 1.435(2); N(1)-C(31), 1.418(2); C(10)-B(1), 1.575(3); C(19)-C(20), 1.394(2); C(19)-C(30), 1.398(3); C(19)-B(1), 1.563(2); C(1)-B(1), 1.577(3). Bond angles (deg): C(32)-Se(1)-C(38), 95.68(8); C(37)-N(1)-C(26), 117.95(15); C(37)-N(1)-C(31), 123.53(15); C(31)-N(1)-C(26), 116.84(14); C(11)-C(10)-B(1), 121.34(15); C(15)-C(10)-B(1), 120.77(16); C(20)-C(19)-C(30), 116.45(16); C(20)-C(19)-B(1), 122.29(15); C(30)-C(19)-B(1), 121.23(16); C(38)-C(37)-N(1), 121.20(19); C(42)-C(37)-N(1), 121.12(18); C(42)-C(37)-C(38), 117.63(19); C(2)-C(1)-B(1), 120.82(16); C(6)-C(1)-C(2), 117.31(17); C(6)-C(1)-B(1), 121.85(15); C(25)-C(26)-N(1), 118.76(16).

Table S3. Crystallographic experimental details for compound **4c** (CCDC 2463490).

Identification code	4c
Empirical formula	$C_{42}H_{38}BNSe$
Formula weight	646.50
Temperature/K	301.15
Crystal system	monoclinic
Space group	$P2_1/c$
a/Å	17.6929(3)
b/Å	9.60560(10)
c/Å	21.6101(4)
α/°	90
β/°	109.558(2)
γ/°	90
Volume/Å^3	3460.75(10)
Z	4
ρ_{calc}g/cm^3	1.241
μ/mm^{-1}	1.678
F(000)	1344.0
Crystal size/mm^3	0.15 × 0.12 × 0.1
Radiation	Cu Kα (λ = 1.54184)
2Θ range for data collection/°	5.3 to 153.556
Index ranges	$-22 \leq h \leq 17$, $-9 \leq k \leq 11$, $-27 \leq l \leq 26$
Reflections collected	26271
Independent reflections	7014 [R_{int} = 0.0273, R_{sigma} = 0.0251]
Data/restraints/parameters	7014/0/412
Goodness-of-fit on F^2	1.039
Final R indexes [I>=2σ (I)]	R_1 = 0.0389, wR_2 = 0.1117
Final R indexes [all data]	R_1 = 0.0466, wR_2 = 0.1180
Largest diff. peak/hole / e Å^{-3}	0.39/-0.56

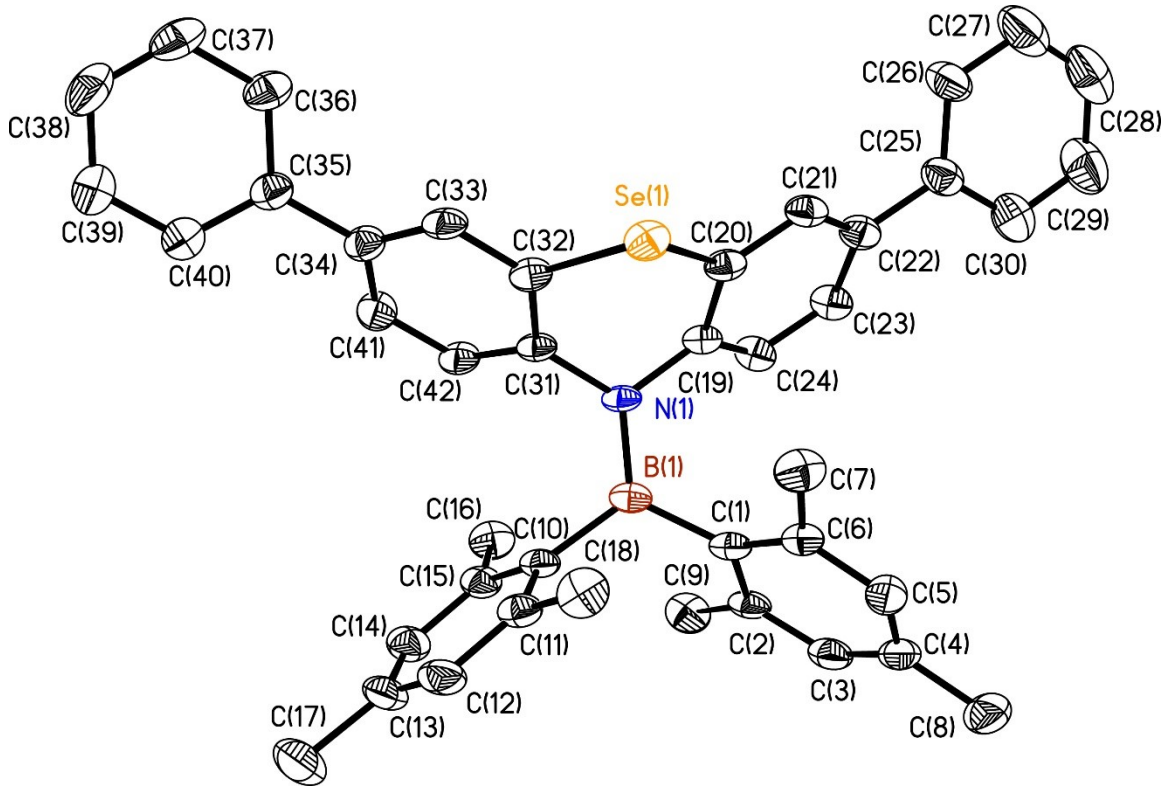

Figure S4. Molecular Structure of **4d** (CCDC 2488434) with thermal ellipsoids presented at a 50% probability level. All hydrogen atoms have been omitted for clarity. Selected bond lengths (Å): Se(1)-C(32), 1.899(6); Se(1)-C(20), 1.893(6); N(1)-C(31), 1.438(7); N(1)-C(19), 1.454(7); N(1)-B(1), 1.424(7); C(31)-C(32), 1.424(8); C(31)-C(42), 1.382(8);C(1)-C(2), 1.434(8); C(1)-C(6), 1.406(9); C(1)-B(1), 1.593(9). Bond angles (deg): C(20)-Se(1)-C(32), 93.9(3); C(31)-N(1)-C(19), 113.6(4); B(1)-N(1)-C(31), 125.9(5); B(1)-N(1)-C(19), 120.4(5); C(32)-C(31)-N(1), 120.8(5); C(42)-C(31)-N(1), 123.0(5); C(42)-C(31)-C(32), 116.1(5); C(2)-C(1)-B(1), 119.6(6); C(6)-C(1)-C(2), 116.1(6); C(6)-C(1)-B(1), 124.1(5); C(31)-C(32)-Se(1), 118.9(4) ;C(33)-C(32)-Se(1), 120.2(4); C(33)-C(32)-C(31), 120.9(6); C(20)-C(19)-N(1), 119.7(5); C(24)-C(19)-N(1), 120.7(5);C(11)-C(10)-C(15), 117.4(6); N(1)-B(1)-C(1), 121.1(5); C(11)-C(10)-B(1), 117.6(6); N(1)-B(1)-C(10), 120.1(5); C(15)-C(10)-B(1), 125.0(5); C(1)-B(1)-C(10), 118.3(5).

Table S4. Crystallographic experimental details for compound **4d** (CCDC 2488 434).

Identification code	4d
Empirical formula	$C_{42}H_{38}BNSe$
Formula weight	646.50
Temperature/K	301.15
Crystal system	Monoclinic
Space group	$P2_1/c$
a/Å	27.5084(7)
b/Å	15.1711(3)
c/Å	8.0954(2)
α/°	90
β/°	91.828(2)
γ/°	90
Volume/Å^3	3376.76(14)
Z	4
ρ_{calc}g/cm^3	1.272
μ/mm^{-1}	1.719
F(000)	1344.0
Crystal size/mm^3	0.12 × 0.11 × 0.1
Radiation	CuKα (λ = 1.54184)
2Θ range for data collection/°	6.43 to 154.282
Index ranges	$-34 \leq h \leq 34$, $-19 \leq k \leq 7$, $-9 \leq l \leq 10$
Reflections collected	23779
Independent reflections	6817 [R_{int} = 0.1202, R_{sigma} = 0.0664]
Data/restraints/parameters	6817/0/413
Goodness-of-fit on F^2	1.116
Final R indexes [I>=2σ (I)]	R_1 = 0.1048, wR_2 = 0.2709
Final R indexes [all data]	R_1 = 0.1243, wR_2 = 0.2790
Largest diff. peak/hole / e Å^{-3}	1.12/-0.83

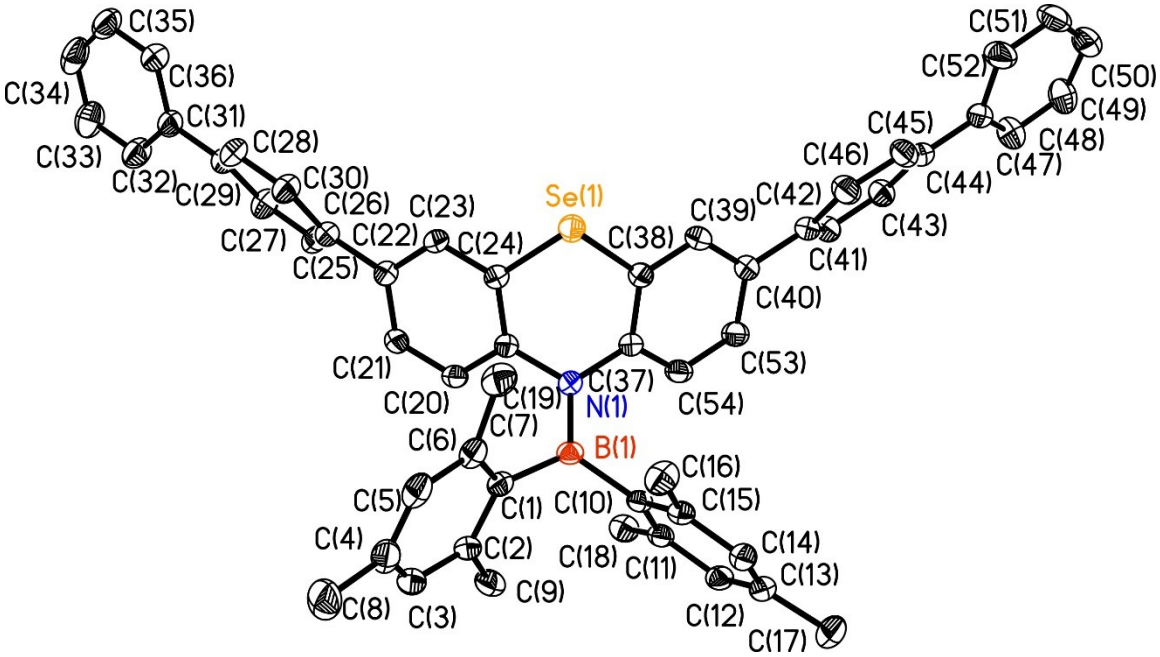

Figure S5. Molecular Structure of **4e** (CCDC 2488435) with thermal ellipsoids presented at a 50% probability level. All hydrogen atoms have been omitted for clarity. Selected bond lengths (Å): Se(1)-C(24), 1.908(3); Se(1)-C(38), 1.911(4); N(1)-C(19), 1.441(4); N(1)-C(37), 1.449(4); N(1)-B(1), 1.433(5); C(20)-C(19), 1.386(5); C(20)-C(21), 1.379(5); C(10)-C(11), 1.412(5); C(10)-C(15), 1.404(5); C(10)-B(1), 1.599(5). Bond angles (deg): C(24)-Se(1)-C(38), 92.89(15); C(19)-N(1)-C(37), 113.3(3); B(1)-N(1)-C(19), 121.1(3); B(1)-N(1)-C(37), 125.7(3); C(21)-C(20)-C(19), 121.0(3); C(11)-C(10)-B(1), 123.1(3); C(15)-C(10)-C(11), 117.5(3); C(15)-C(10)-B(1), 119.3(3); C(20)-C(19)-N(1), 119.9(3); C(20)-C(19)-C(24), 118.2(3); C(24)-C(19)-N(1), 121.8(3); C(19)-C(24)-Se(1), 118.9(3); C(19)-C(24)-C(23), 121.0(3); C(23)-C(24)-Se(1), 120.0(2); C(2)-C(1)-C(6), 116.6(3); C(2)-C(1)-B(1), 121.9(3); C(6)-C(1)-B(1), 120.9(3); C(10)-B(1)-C(1), 118.0(3).

Table S5. Crystallographic experimental details for compound **4e** (CCDC 2488435).

Identification code	4e
Empirical formula	$C_{54}H_{46}BNSe$
Formula weight	798.69
Temperature/K	301.37(10)
Crystal system	Orthorhombic
Space group	$P2_12_12_1$
a/Å	10.6317(2)
b/Å	12.3024(3)
c/Å	32.1027(6)
α/°	90
β/°	90
γ/°	90
Volume/Å^3	4198.89(15)
Z	4
ρ_{calc}g/cm^3	1.263
μ/mm^{-1}	1.486
F(000)	1664.0
Crystal size/mm^3	0.13 × 0.12 × 0.1
Radiation	Cu Kα (λ = 1.54184)
2Θ range for data collection/°	5.506 to 153.812
Index ranges	$-12 \leq h \leq 6$, $-15 \leq k \leq 15$, $-40 \leq l \leq 33$
Reflections collected	17027
Independent reflections	7732 [R_{int} = 0.0396, R_{sigma} = 0.0437]
Data/restraints/parameters	7732/63/539
Goodness-of-fit on F^2	1.024
Final R indexes [I>=2σ (I)]	R_1 = 0.0389, wR_2 = 0.0960
Final R indexes [all data]	R_1 = 0.0481, wR_2 = 0.1013
Largest diff. peak/hole / e Å^{-3}	0.28/-0.37
Flack parameter	-0.011(12)

4. The excitation and emission spectra

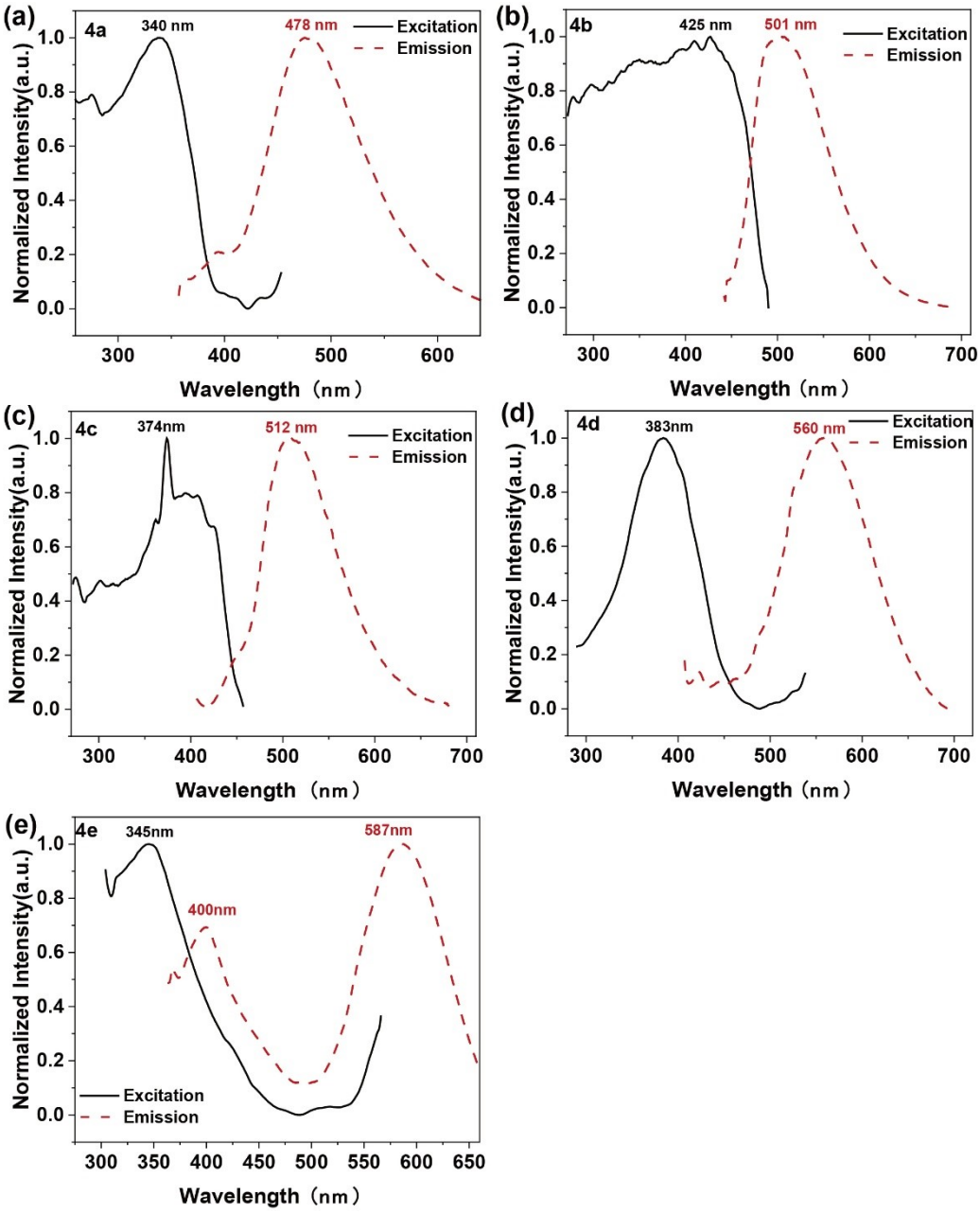

Figure S6. Fluorescence excitation (solid line) and emission spectra (dashed line) of **3a**.

5. The fluorescence lifetime decay spectra

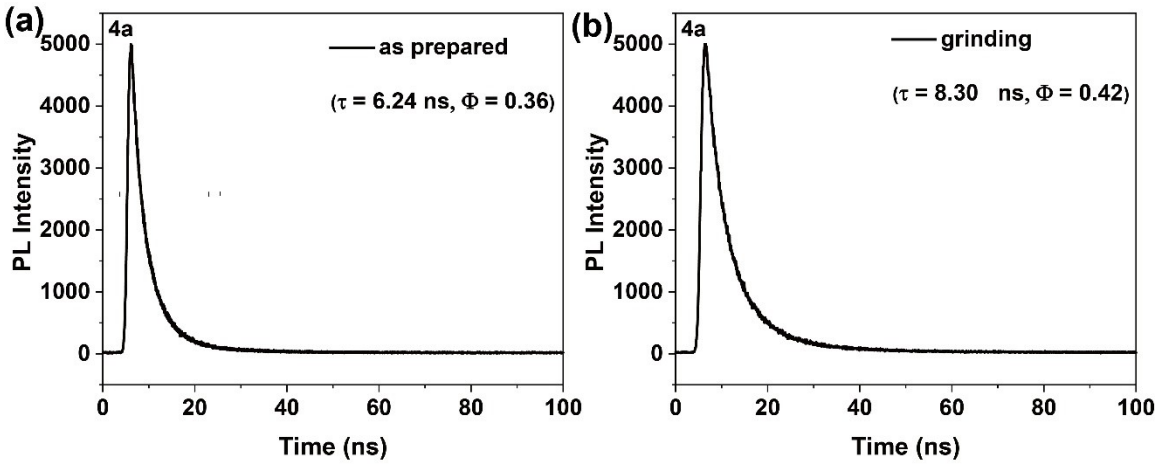

Figure S7. Fluorescence lifetime decay spectra of **4a**.

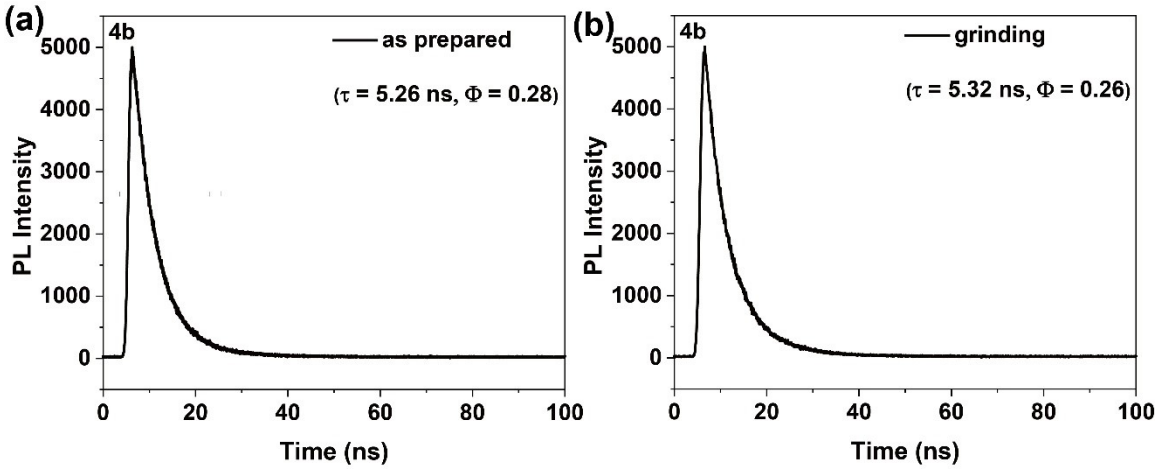

Figure S8. Fluorescence lifetime decay spectra of **4b**.

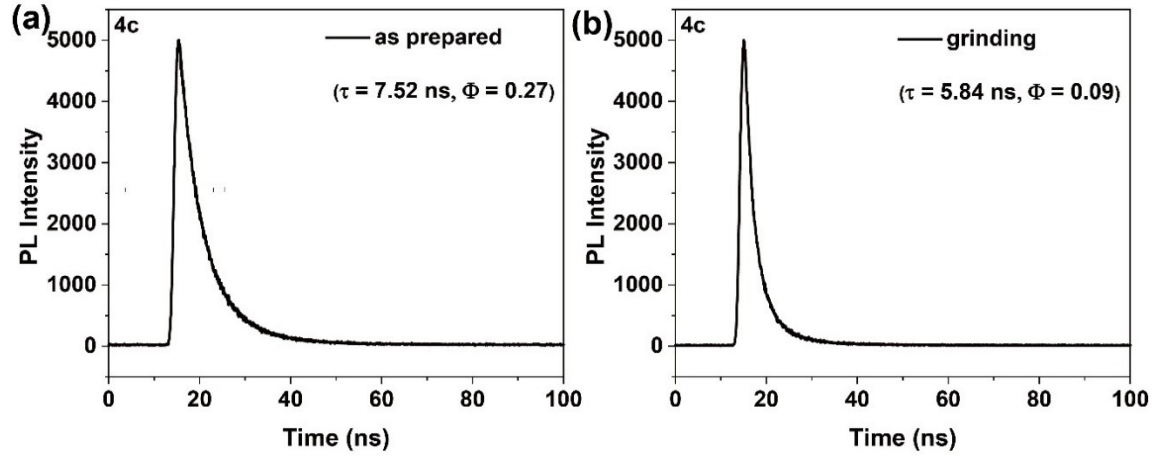

Figure S9. Fluorescence lifetime decay spectra of **4c**.

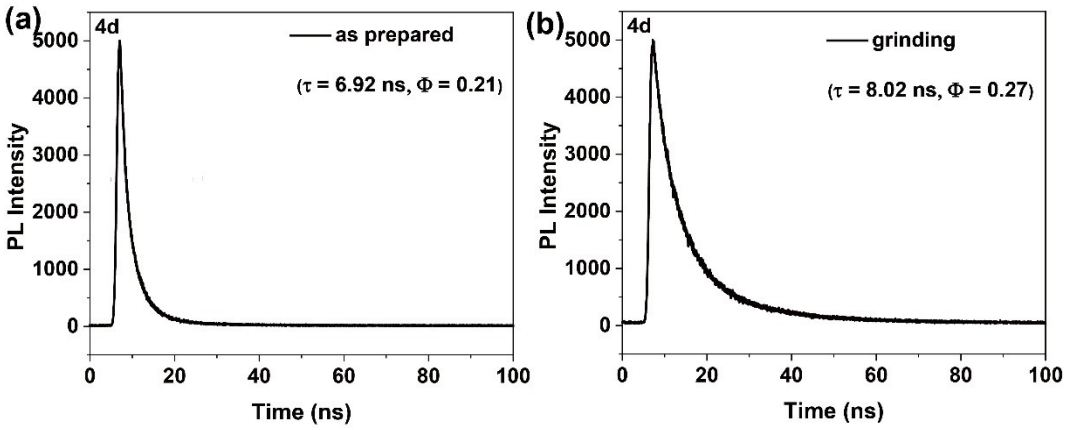

Figure S10. Fluorescence lifetime decay spectra of **4d**.

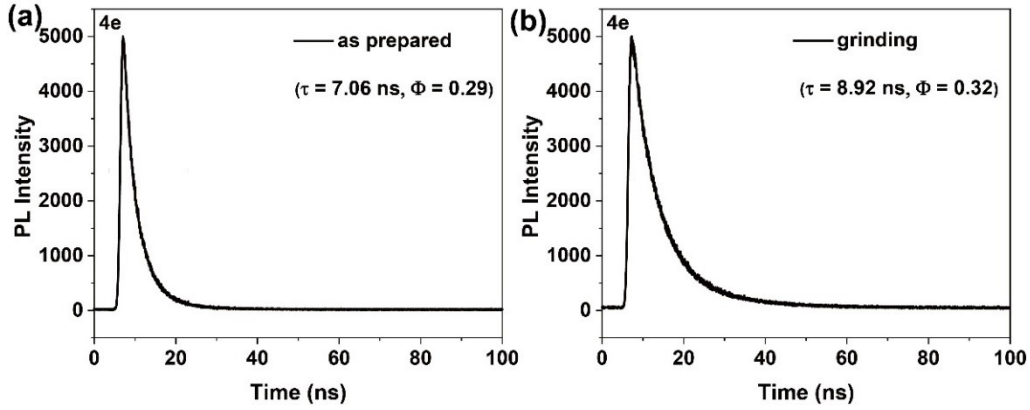

Figure S11. Fluorescence lifetime decay spectra of **4e**.

6. The Experimental and the Calculated UV-Vis spectra

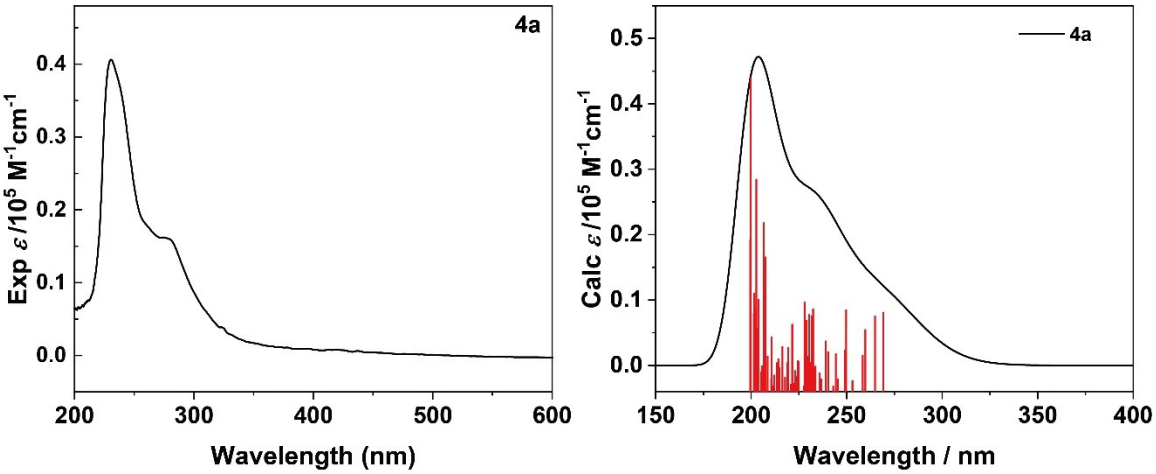

Figure S12. Computed, at the TD-DFT, B3LYP-D3/6-31g(d)[3-6], scrf = (solvent = THF), level of theory and experimental UV-vis spectra of **4a**.

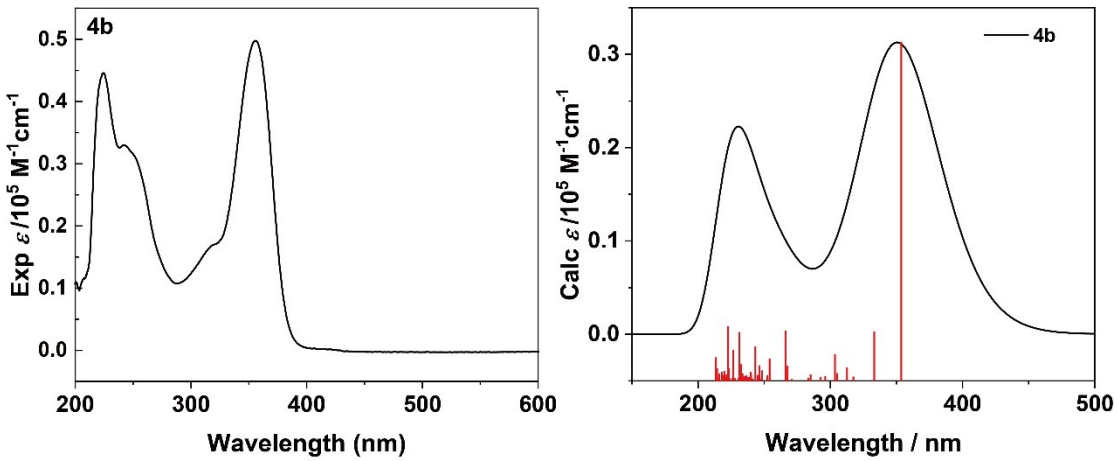

Figure S13. Computed, at the TD-DFT, B3LYP-D3/6-31g(d), scrf = (solvent = THF), level of theory and experimental UV-vis spectra of **4b**.

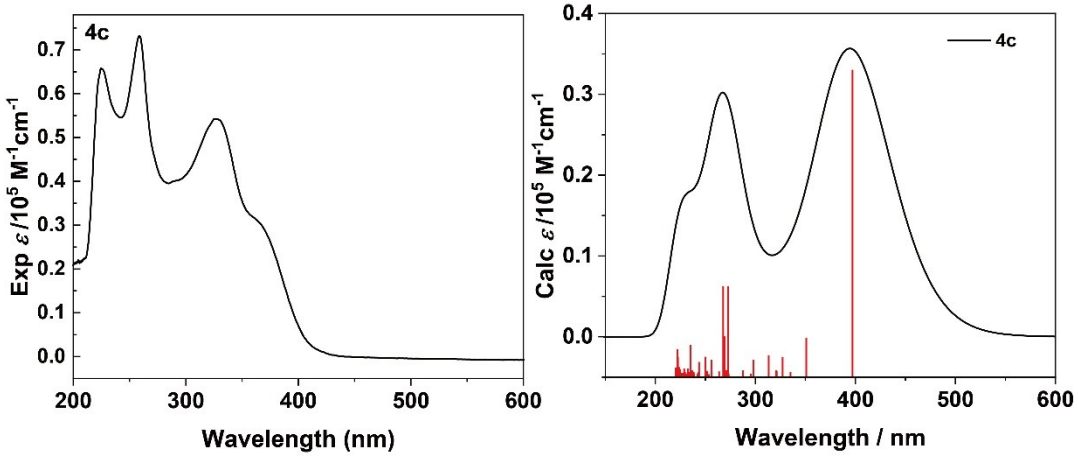

Figure S14. Computed, at the TD-DFT, B3LYP-D3/6-31g(d), scrf = (solvent = THF), level of theory and experimental UV-vis spectra of **4c**.

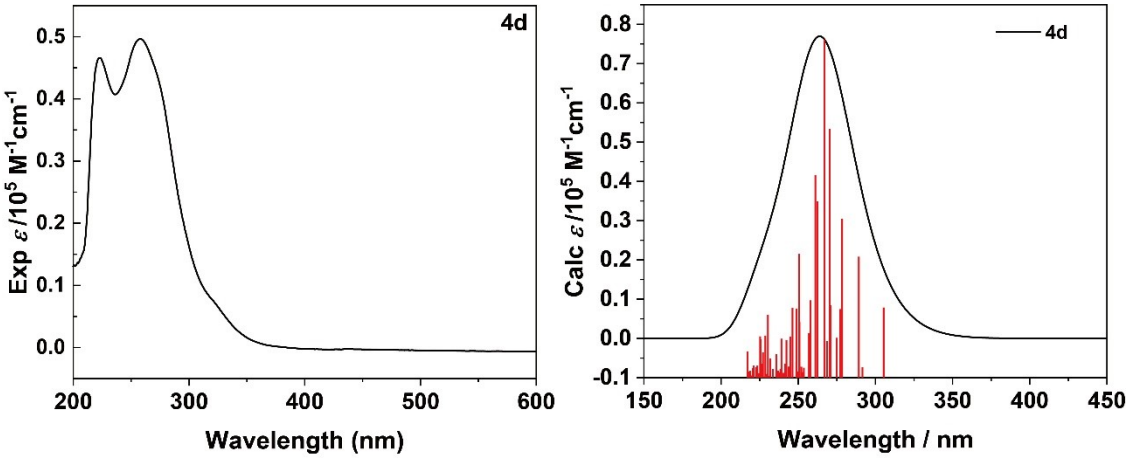

Figure S15. Computed, at the TD-DFT, B3LYP-D3/6-31g(d), scrf = (solvent = THF), level of theory and experimental UV-vis spectra of **4d**.

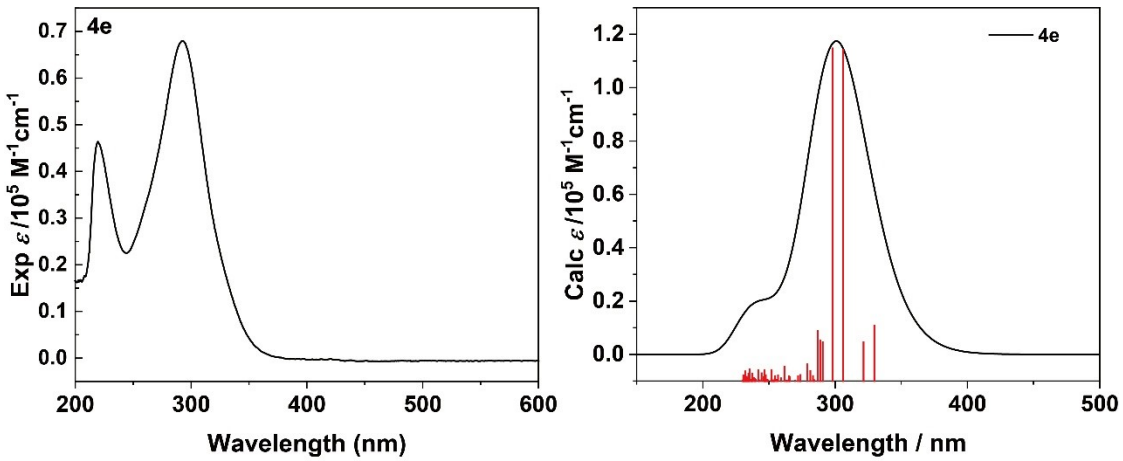

Figure S16. Computed, at the TD-DFT, B3LYP-D3/6-31g(d, p), scrf = (solvent = THF) level of theory and experimental UV-vis spectra of **4e**.

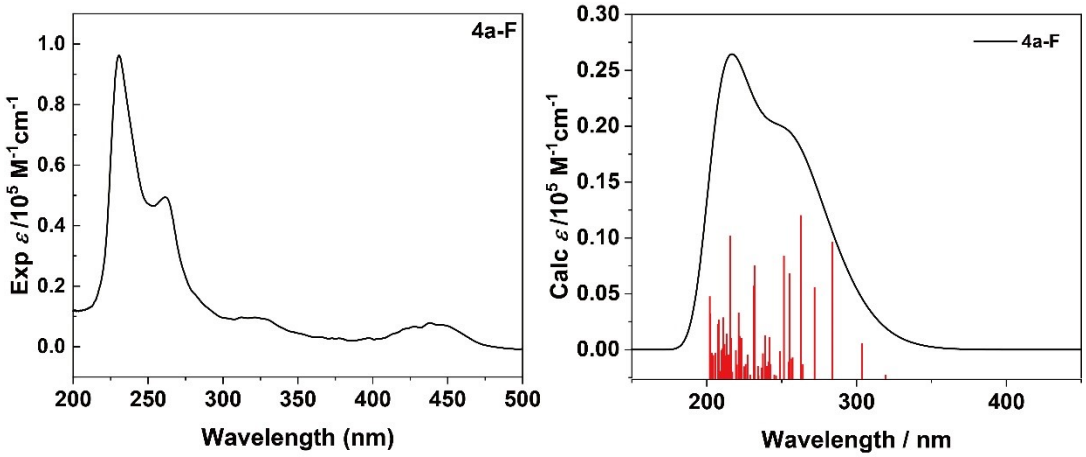

Figure S17 Computed, at the TD-DFT, B3LYP-D3/6-31g(d, p), scrf = (solvent = THF) level of theory and experimental UV-vis spectra of **4a-F**.

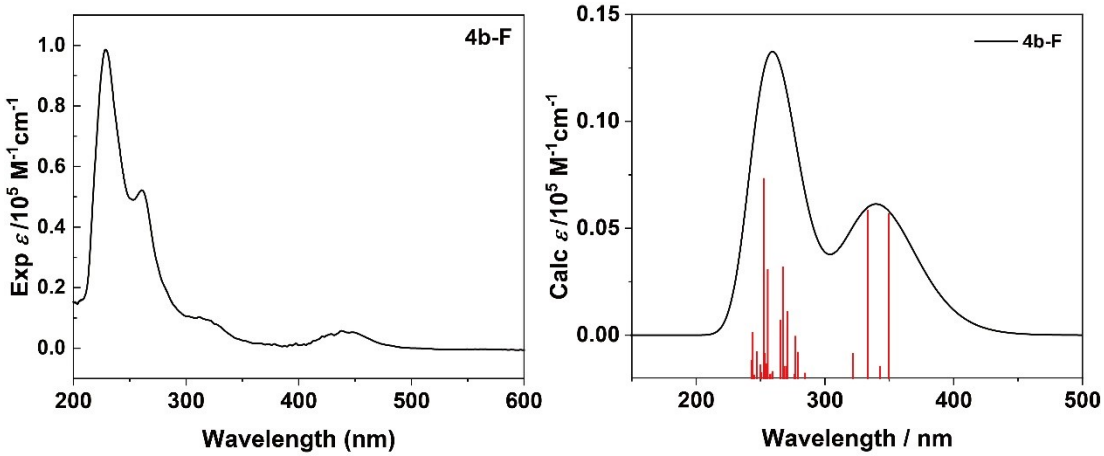

Figure S18. Computed, at the TD-DFT, B3LYP-D3/6-31g(d, p), scrf = (solvent = THF) level of theory and experimental UV-vis spectra of **4b-F**.

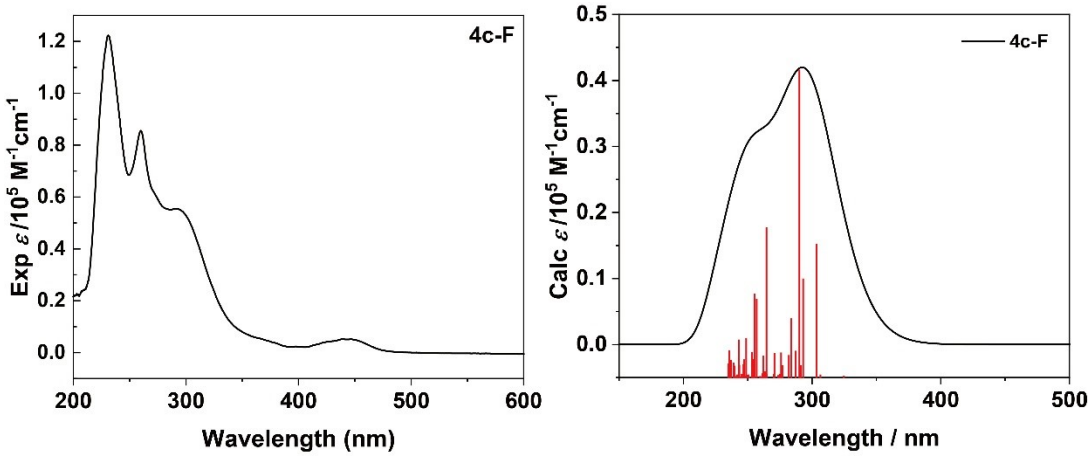

Figure S19. Computed, at the TD-DFT, B3LYP-D3/6-31g(d, p), scrf = (solvent = THF) level of theory and experimental UV-vis spectra of **4c-F**.

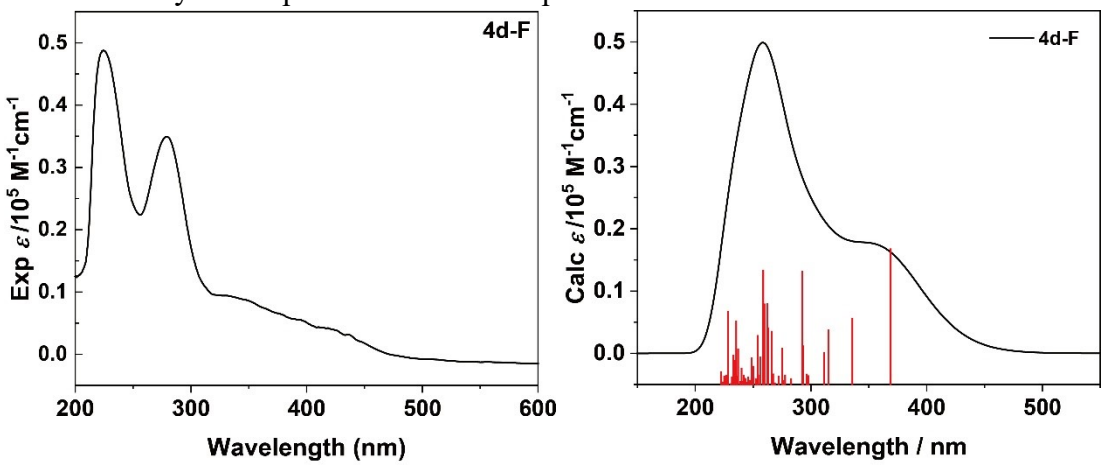

Figure S20. Computed, at the TD-DFT, B3LYP-D3/6-31g(d, p), scrf = (solvent = THF) level of theory and experimental UV-vis spectra of **4d-F**.

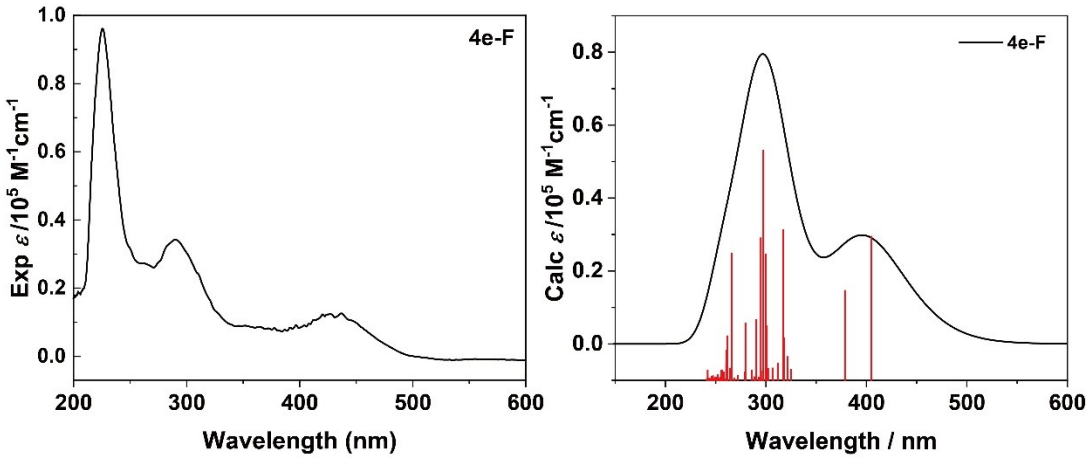

Figure S21. Computed, at the TD-DFT, B3LYP-D3/6-31g(d, p), scrf = (solvent = THF) level of theory and experimental UV-vis spectra of **4e-F**.

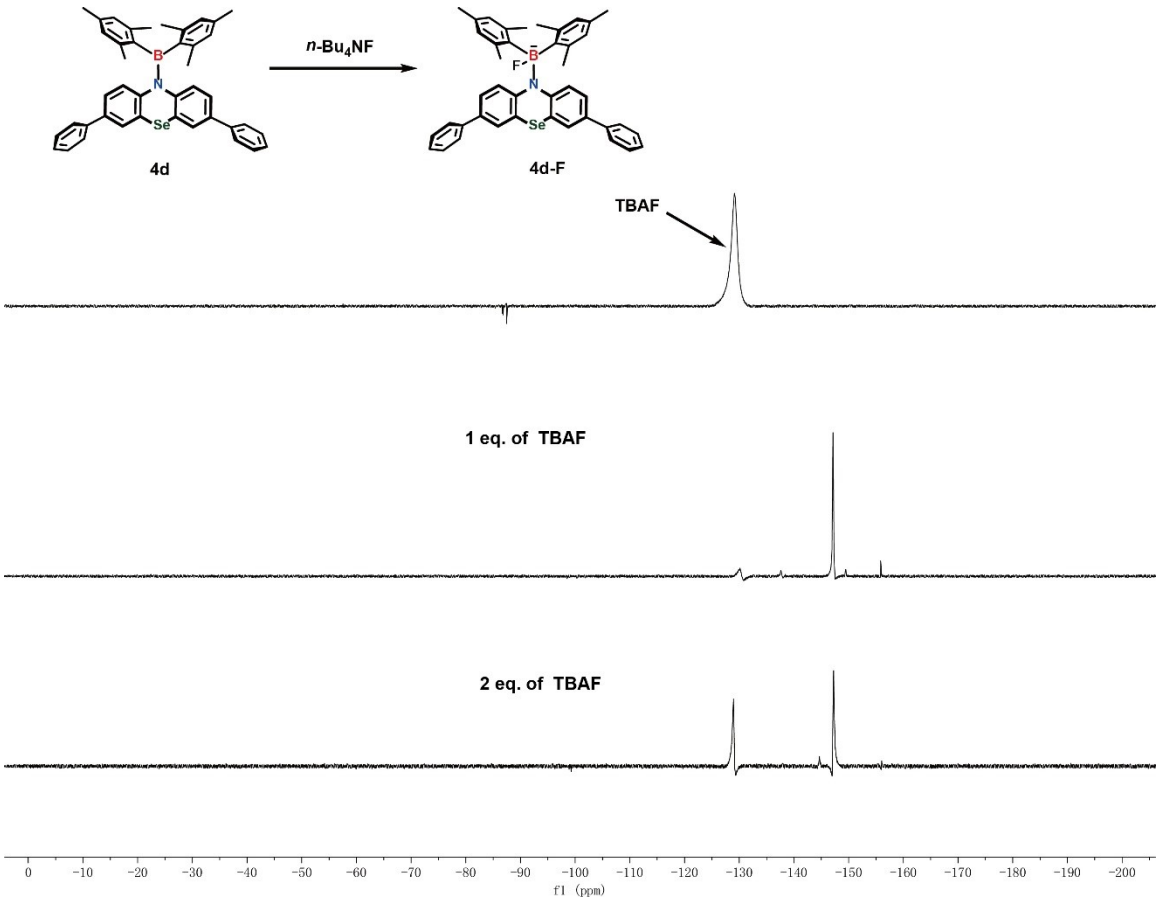

Figure S22. (top) Fluoride anion binding to model compound **4d**. (bottom) ^{19}F NMR spectra of a mixture of **4d** after addition of TBAF.

Table S6 Photophysical data for **4a**-**4e**.

Comp.	λ_{abs1}[a] (nm)	λ_{abs2}[a] (nm)	λ_{em}[b] (nm)	SS_1[c] (cm^{-1})	SS_2[c] (cm^{-1})	τ[d] (ns)	QY[e] (%)
4a	230	278	478	22558	15051	6.24	36
4b	225	356	488	23953	7598	5.26	28
4c	226	327	522	25091	11424	7.52	27
4d	223	259	564	27113	20880	6.92	21
4e	222	294	587	28009	16978	7.06	29

[a] The λ_{max} values in the UV-vis spectra.[b] Emission maxima in THF. [c] Stokes shift = $1/\lambda_{abs} - 1/\lambda_{em}$.[d] Lifetimes in the solid state. [e] Quantum yield in the solid state.

Table S7 Calculated ($\lambda_{TD\text{-}DFT}$) wavelengths of **4a**. Molecular orbitals (MOs) involved in the main electronic transition，f corresponds to the oscillator strength. (TD-DFT, B3LYP/6-31g(d, p))

$\lambda_{TD\text{-}DFT}$	Oscillator Strength, f	MOs	
281.56	0.0555	HOMO ->LUMO	64.93%
		HOMO ->LUMO+1	10.14%
		HOMO ->LUMO+2	19.75%
276.42	0.0526	HOMO ->LUMO	12.41%
		HOMO ->LUMO+1	38.87%
		HOMO ->LUMO+2	52.33%
		HOMO ->LUMO+8	15.21%
258.33	0.0572	HOMO-4 ->LUMO	20.15%
		HOMO-3 ->LUMO	45.16%
		HOMO-2 ->LUMO	14.11%
		HOMO-1 ->LUMO+1	11.62%
		HOMO ->LUMO+3	29.77%
		HOMO ->LUMO+4	26.78%
245.50	0.0351	HOMO-4 ->LUMO+2	10.59%
		HOMO-3 ->LUMO	12.10%
		HOMO-3 ->LUMO+1	10.44%
		HOMO-2 ->LUMO+1	19.77%
		HOMO-2 ->LUMO+3	14.59%
		HOMO-1 ->LUMO+1	14.92%
		HOMO-1 ->LUMO+2	49.09%
		HOMO-1 ->LUMO+3	16.04%
		HOMO-1 ->LUMO+6	13.41%
237.54	0.0577	HOMO-4 ->LUMO+1	27.11%
		HOMO-4 ->LUMO+2	18.19%
		HOMO-2 ->LUMO+2	45.97%
		HOMO-1 ->LUMO+3	31.01%
		HOMO-1 ->LUMO+4	12.78%
232.13	0.0626	HOMO-5 ->LUMO	48.50%
		HOMO-4 ->LUMO+2	23.61%
		HOMO-3 ->LUMO+5	12.01%
		HOMO-2 ->LUMO+2	15.36%
		HOMO-1 ->LUMO+3	10.64%
		HOMO ->LUMO+5	21.47%
		HOMO ->LUMO+8	15.40%

Table S8. Calculated ($\lambda_{TD\text{-}DFT}$) wavelengths of **4b**. Molecular orbitals (MOs) involved in the main electronic transition，f corresponds to the oscillator strength. (TD-DFT, B3LYP/6-31g(d, p))

$\lambda_{TD\text{-}DFT}$	Oscillator Strength, f	MOs	
354.14	0.6782	HOMO-4 ->LUMO	10.62%
		HOMO-3 ->LUMO	11.01%
		HOMO ->LUMO	67.69%
333.77	0.0952	HOMO-2 ->LUMO	69.91%
		HOMO-1 ->LUMO	47.68%
266.55	0.0980	HOMO-4 ->LUMO+2	10.10%
		HOMO-1 ->LUMO+2	59.25%
		HOMO-1 ->LUMO+4	16.31%
		HOMO-1 ->LUMO+9	17.94%
		HOMO ->LUMO+2	10.89%
		HOMO ->LUMO+4	12.62%
		HOMO ->LUMO+9	14.42%
232.92	0.0301	HOMO-10 ->LUMO	12.79%
		HOMO-5 ->LUMO+1	36.24%
		HOMO-5 ->LUMO+5	13.86%
		HOMO-4 ->LUMO+2	14.13%
		HOMO-4 ->LUMO+3	21.08%
		HOMO-4 ->LUMO+4	10.30%
		HOMO-3 ->LUMO+2	10.08%
		HOMO-3 ->LUMO+3	13.40%
		HOMO-2 ->LUMO+7	13.80%
		HOMO ->LUMO+8	33.83%
232.51	0.0246	HOMO-7 ->LUMO+3	10.27%
		HOMO-1 ->LUMO+6	26.49%
		HOMO-1 ->LUMO+7	19.35%
		HOMO-1 ->LUMO+9	40.74%
		HOMO ->LUMO+8	16.35%
		HOMO ->LUMO+9	28.00%
214.05	0.0441	HOMO-8 ->LUMO+1	13.35%
		HOMO-8 ->LUMO+3	13.77%
		HOMO-7 ->LUMO+1	42.24%
		HOMO-7 ->LUMO+3	38.94%
		HOMO-6 ->LUMO+3	23.50%
		HOMO-1 ->LUMO+8	26.27%

Table S9. Calculated ($\lambda_{TD\text{-}DFT}$) wavelengths of **4c**. Molecular orbitals (MOs) involved in the main electronic transition，f corresponds to the oscillator strength. (TD-DFT, B3LYP/6-31g(d, p))

$\lambda_{TD\text{-}DFT}$	Oscillator Strength, f	MOs	
397.41	0.8377	HOMO ->LUMO	69.44%
298.57	0.0405	HOMO-1 ->LUMO+1	10.89%
		HOMO ->LUMO+2	28.96%
		HOMO ->LUMO+3	60.71%
		HOMO ->LUMO+5	11.77%
272.85	0.2428	HOMO-6 ->LUMO	57.58%
		HOMO-1 ->LUMO+1	32.19%
		HOMO ->LUMO+5	13.50%
269.51	0.1049	HOMO-1 ->LUMO+2	52.49%
		HOMO-1 ->LUMO+3	25.92%
		HOMO-1 ->LUMO+4	20.37%
		HOMO-1 ->LUMO+11	19.80%
		HOMO ->LUMO+11	14.47%
268.14	0.2431	HOMO-1 ->LUMO+1	25.76%
		HOMO ->LUMO+5	62.54%
235.30	0.0812	HOMO-13 ->LUMO	31.70%
		HOMO-12 ->LUMO	15.30%
		HOMO-11 ->LUMO	29.74%
		HOMO-4 ->LUMO+1	18.59%
		HOMO-1 ->LUMO+5	13.75%
		HOMO ->LUMO+10	41.62%
222.81	0.0479	HOMO-6 ->LUMO+1	21.11%
		HOMO-5 ->LUMO+3	14.80%
		HOMO-5 ->LUMO+7	11.28%
		HOMO-4 ->LUMO+5	14.86%
		HOMO-4 ->LUMO+6	10.90%
		HOMO-4 ->LUMO+7	16.92%
		HOMO-3 ->LUMO+6	11.14%
		HOMO-3 ->LUMO+7	22.97%
		HOMO-2 ->LUMO+7	17.46%
		HOMO-1 ->LUMO+6	10.06%
		HOMO-1 ->LUMO+7	10.11%
		HOMO-1 ->LUMO+8	16.57%
		HOMO ->LUMO+12	30.28%

Table S10. Calculated ($\lambda_{TD\text{-}DFT}$) wavelengths of **4d**. Molecular orbitals (Mos) involved in the main electronic transition，f corresponds to the oscillator strength. (TD-DFT, B3LYP/6-31g(d, p))

$\lambda_{TD\text{-}DFT}$	Oscillator Strength, f	MOs	
305.18	0.0780	HOMO ->LUMO	67.86%
291.52	0.0098	HOMO ->LUMO+1	67.77%
289.19	0.1358	HOMO-1 ->LUMO	66.54%
		HOMO ->LUMO+2	11.08%
278.33	0.1790	HOMO-4 ->LUMO	12.25%
		HOMO-3 ->LUMO	38.84%
		HOMO-1 ->LUMO	16.93%
		HOMO-1 ->LUMO+1	21.11%
		HOMO ->LUMO+2	37.84%
		HOMO ->LUMO+3	25.03%
		HOMO ->LUMO+4	10.11%
270.16	0.2814	HOMO-4 ->LUMO	31.60%
		HOMO-3 ->LUMO	39.43%
		HOMO-2 ->LUMO+1	11.20%
		HOMO-1 ->LUMO+1	31.17%
		HOMO ->LUMO+2	26.45%
		HOMO ->LUMO+3	14.89%
266.97	0.3826	HOMO-5 ->LUMO	67.38%
262.37	0.1986	HOMO-6 ->LUMO	12.48%
		HOMO-6 ->LUMO+1	11.96%
		HOMO-4 ->LUMO+1	14.33%
		HOMO-3 ->LUMO+1	50.99%
		HOMO-3 ->LUMO+3	10.56%
		HOMO-2 ->LUMO+1	21.60%
		HOMO-1 ->LUMO+1	18.17%
		HOMO-1 ->LUMO+2	13.69%
		HOMO-1 ->LUMO+4	10.54%
260.97	0.2286	HOMO-6 ->LUMO	58.34%
		HOMO-3 ->LUMO	10.06%
		HOMO-3 ->LUMO+1	13.21%
		HOMO-1 ->LUMO+1	10.25%
		HOMO-1 ->LUMO+2	15.86%
		HOMO ->LUMO+2	14.48%

Table S11. Calculated ($\lambda_{TD\text{-}DFT}$) wavelengths of **4e**. Molecular orbitals (MOs) involved in the main electronic transition，f corresponds to the oscillator strength. (TD-DFT, B3LYP/6-31g(d, p))

$\lambda_{TD\text{-}DFT}$	Oscillator Strength, f	MOs	
329.76	0.1919	HOMO ->LUMO	67.99%
		HOMO ->LUMO+3	10.04%
290.80	0.1351	HOMO-3 ->LUMO	14.44%
		HOMO-2 ->LUMO	29.27%
		HOMO-2 ->LUMO+1	48.91%
		HOMO-1 ->LUMO	32.18%
288.84	0.1400	HOMO-3 ->LUMO	19.62%
		HOMO-2 ->LUMO	19.77%
		HOMO-1 ->LUMO+1	60.31%
		HOMO ->LUMO+2	14.95%
287.34	0.1741	HOMO-4 ->LUMO	17.86%
		HOMO-3 ->LUMO	45.51%
		HOMO-2 ->LUMO	21.49%
		HOMO-2 ->LUMO+1	20.29%
		HOMO-1 ->LUMO+1	10.81%
		HOMO ->LUMO+2	21.57%
		HOMO ->LUMO+4	24.08%
235.62	0.0403	HOMO-13 ->LUMO	15.75%
		HOMO-9 ->LUMO	17.02%
		HOMO-9 ->LUMO+1	16.28%
		HOMO-8 ->LUMO	10.99%
		HOMO-2 ->LUMO+5	13.15%
		HOMO-2 ->LUMO+7	11.61%
		HOMO-1 ->LUMO+5	21.50%
		HOMO-1 ->LUMO+6	11.66%
		HOMO-1 ->LUMO+7	25.21%
		HOMO ->LUMO+12	30.76%

Table S12. Calculated ($\lambda_{TD\text{-}DFT}$) wavelengths of **4a-F**. Molecular orbitals (MOs) involved in the main electronic transition，f corresponds to the oscillator strength. (TD-DFT, B3LYP/6-31g(d, p))

$\lambda_{TD\text{-}DFT}$	Oscillator Strength, f	MOs	
304.08	0.0235	HOMO ->LUMO	39.52%
		HOMO ->LUMO+1	56.70%
284.41	0.0933	HOMO ->LUMO+2	60.82%
		HOMO ->LUMO+3	27.34%
		HOMO ->LUMO+4	13.27%
263.16	0.1116	HOMO-4 ->LUMO	12.98%
		HOMO-4 ->LUMO+1	10.19%
		HOMO-2 ->LUMO	29.07%
		HOMO-2 ->LUMO+1	22.49%
		HOMO ->LUMO+3	20.79%
		HOMO ->LUMO+4	15.98%
		HOMO ->LUMO+6	35.48%
		HOMO ->LUMO+7	16.99%
		HOMO ->LUMO+8	22.04%
255.77	0.0717	HOMO-4 ->LUMO+1	13.21%
		HOMO-2 ->LUMO	19.26%
		HOMO-2 ->LUMO+1	14.50%
		HOMO-1 ->LUMO	30.55%
		HOMO-1 ->LUMO+1	34.21%
		HOMO ->LUMO+5	28.75%
		HOMO ->LUMO+6	25.89%
		HOMO ->LUMO+8	10.45%
252.00	0.0835	HOMO-4 ->LUMO+1	12.39%
		HOMO-3 ->LUMO+1	11.22%
		HOMO-2 ->LUMO	26.92%
		HOMO-2 ->LUMO+1	48.56%
		HOMO-1 ->LUMO	15.76%
		HOMO-1 ->LUMO+1	17.19%
		HOMO-1 ->LUMO+2	16.39%

Table S13. Calculated ($\lambda_{TD\text{-}DFT}$) wavelengths of **4b-F**. Molecular orbitals (MOs) involved in the main electronic transition，f corresponds to the oscillator strength. (TD-DFT, B3LYP/6-31g(d, p))

$\lambda_{TD\text{-}DFT}$	Oscillator Strength, f	MOs	
334.05	0.0768	HOMO ->LUMO+2	69.72%
271.84	0.0273	HOMO-5 ->LUMO+1	50.54%
		HOMO-5 ->LUMO+4	10.23%
		HOMO-2 ->LUMO+1	21.47%
		HOMO-1 ->LUMO+3	13.47%
		HOMO ->LUMO+4	27.82%
		HOMO ->LUMO+5	20.30%
271.41	0.0206	HOMO-5 ->LUMO	62.19%
		HOMO-2 ->LUMO+1	23.50%
256.41	0.0448	HOMO-5 ->LUMO+2	65.17%
		HOMO-3 ->LUMO+1	12.58%
		HOMO-3 ->LUMO+2	10.62%
253.21	0.0361	HOMO-4 ->LUMO+1	41.19%
		HOMO-4 ->LUMO+2	20.22%
		HOMO-3 ->LUMO+2	35.17%
		HOMO ->LUMO+6	37.90%
247.91	0.0109	HOMO-7 ->LUMO	27.72%
		HOMO-6 ->LUMO	48.48%
		HOMO-1 ->LUMO+7	10.85%
		HOMO ->LUMO+5	10.11%
		HOMO ->LUMO+7	21.48%
		HOMO ->LUMO+8	20.05%
		HOMO ->LUMO+9	10.53%
244.81	0.0188	HOMO-6 ->LUMO	20.36%
		HOMO-4 ->LUMO+3	12.20%
		HOMO-4 ->LUMO+6	14.51%
		HOMO-3 ->LUMO+3	26.99%
		HOMO-1 ->LUMO+6	10.38%
		HOMO-1 ->LUMO+7	14.69%
		HOMO ->LUMO+8	38.93%
		HOMO ->LUMO+9	20.22%

Table S14. Calculated ($\lambda_{TD\text{-}DFT}$) wavelengths of **4c-F**. Molecular orbitals (MOs) involved in the main electronic transition，f corresponds to the oscillator strength. (TD-DFT, B3LYP/6-31g(d, p))

$\lambda_{TD\text{-}DFT}$	Oscillator Strength, f	MOs	
312.49	0.2010	HOMO-1 ->LUMO	16.77%
		HOMO ->LUMO	64.78%
		HOMO ->LUMO+1	17.34%
298.90	0.1485	HOMO-3 ->LUMO	25.47%
		HOMO-2 ->LUMO	62.89%
		HOMO-2 ->LUMO+1	16.60%
295.25	0.4646	HOMO-3 ->LUMO	61.69%
		HOMO-2 ->LUMO	23.77%
		HOMO-1 ->LUMO+2	15.23%
250.18	0.1261	HOMO-6 ->LUMO	12.21%
		HOMO-6 ->LUMO+1	60.13%
		HOMO-1 ->LUMO+4	10.33%
		HOMO-1 ->LUMO+7	26.61%
234.62	0.0561	HOMO-8 ->LUMO+1	15.96%
		HOMO-5 ->LUMO+4	12.25%
		HOMO-2 ->LUMO+6	17.50%
		HOMO-2 ->LUMO+8	18.73%
		HOMO-2 ->LUMO+9	10.96%
		HOMO ->LUMO+7	11.51%
		HOMO ->LUMO+8	43.71%
		HOMO ->LUMO+9	23.42%
224.62	0.202	HOMO-9 ->LUMO+1	15.59%
		HOMO-8 ->LUMO+1	13.14%
		HOMO-7 ->LUMO+1	15.53%
		HOMO-7 ->LUMO+3	22.92%
		HOMO-3 ->LUMO+6	12.43%
		HOMO-3 ->LUMO+8	41.29%
		HOMO-2 ->LUMO+7	10.89%
		HOMO-2 ->LUMO+8	18.20%
		HOMO-2 ->LUMO+9	12.97%
		HOMO-2 ->LUMO+10	12.21%
		HOMO ->LUMO+10	16.49%

Table S15. Calculated ($\lambda_{TD\text{-}DFT}$) wavelengths of **4d-F**. Molecular orbitals (MOs) involved in the main electronic transition，f corresponds to the oscillator strength. (TD-DFT, B3LYP/6-31g(d, p))

$\lambda_{TD\text{-}DFT}$	Oscillator Strength, f	MOs	
369.54	0.3147	HOMO ->LUMO	69.05%
		HOMO ->LUMO+5	10.12%
336.35	0.1233	HOMO ->LUMO+1	68.14%
298.41	0.157	HOMO ->LUMO+3	59.99%
		HOMO ->LUMO+5	33.23%
292.93	0.2112	HOMO-4 ->LUMO	17.95%
		HOMO-2 ->LUMO	57.85%
		HOMO-1 ->LUMO	20.69%
		HOMO-1 ->LUMO+1	14.40%
		HOMO ->LUMO+8	10.08%
263.84	0.1054	HOMO-6 ->LUMO	11.82%
		HOMO-5 ->LUMO	55.48%
		HOMO-5 ->LUMO+1	13.92%
		HOMO-4 ->LUMO+1	22.11%
		HOMO-3 ->LUMO+1	25.88%
		HOMO ->LUMO+7	10.12%
263.04	0.1508	HOMO-6 ->LUMO	60.37%
		HOMO-6 ->LUMO+1	12.65%
		HOMO-3 ->LUMO+1	27.02%
260.32	0.1498	HOMO-6 ->LUMO+1	20.96%
		HOMO-5 ->LUMO+1	26.58%
		HOMO-1 ->LUMO+2	47.92%
		HOMO-1 ->LUMO+4	29.93%
		HOMO ->LUMO+7	11.07%
259.39	0.2128	HOMO-6 ->LUMO+1	33.01%
		HOMO-5 ->LUMO	10.69%
		HOMO-5 ->LUMO+1	46.13%
		HOMO-1 ->LUMO+2	26.87%
		HOMO-1 ->LUMO+4	17.29%
		HOMO ->LUMO+7	15.58%

Table S16. Calculated ($\lambda_{TD\text{-}DFT}$) wavelengths of **4e-F**. Molecular orbitals (MOs) involved in the main electronic transition，f corresponds to the oscillator strength. (TD-DFT, B3LYP/6-31g(d, p))

$\lambda_{TD\text{-}DFT}$	Oscillator Strength, f	MOs	
404.00	0.5665	HOMO->LUMO	68.65%
316.32	0.3290	HOMO->LUMO+7	24.03%
		HOMO-4->LUMO+1	10.86%
		HOMO-2->LUMO	43.27%
		HOMO-2->LUMO+1	11.75%
		HOMO-1->LUMO+1	39.42%
		HOMO->LUMO+2	16.89%
		HOMO->LUMO+4	14.05%
		HOMO->LUMO+6	12.55%
299.11	0.2753	HOMO-2->LUMO+1	21.34%
		HOMO-5->LUMO	25.57%
		HOMO-5->LUMO+1	11.97%
		HOMO-4->LUMO	45.39%
		HOMO-4->LUMO+1	24.64%
		HOMO-3->LUMO	29.36%
296.59	0.5036	HOMO-2->LUMO	21.59%
		HOMO-5->LUMO	52.20%
		HOMO-5->LUMO+1	18.78%
294.04	0.3113	HOMO-3->LUMO+1	63.40%
		HOMO-5->LUMO	23.61%
		HOMO-5->LUMO+1	11.96%
		HOMO-4->LUMO	19.83%
		HOMO-4->LUMO+1	54.16%
		HOMO-3->LUMO+1	11.84%
		HOMO->LUMO+6	13.48%
265.12	0.2773	HOMO->LUMO+14	14.32%
		HOMO-7->LUMO	64.21%

7. Electrochemical properties

Cyclic voltammograms were recorded with a Metrohm PGSTAT204 electrochemical analyzer using DCM. The CV cell consisted of a gold electrode, a Pt wire counter electrode, and an Ag/AgCl reference electrode. All measurements were performed using DCM solutions of samples with a concentration of 1 mM and 0.1 M $Bu_4N^+BF_6^-$ as a supporting electrolyte with a scan rate of 10 mVs^{-1}. Potentials are determined against a ferrocene/ferrocenyl ion couple (Fc/Fc^+).

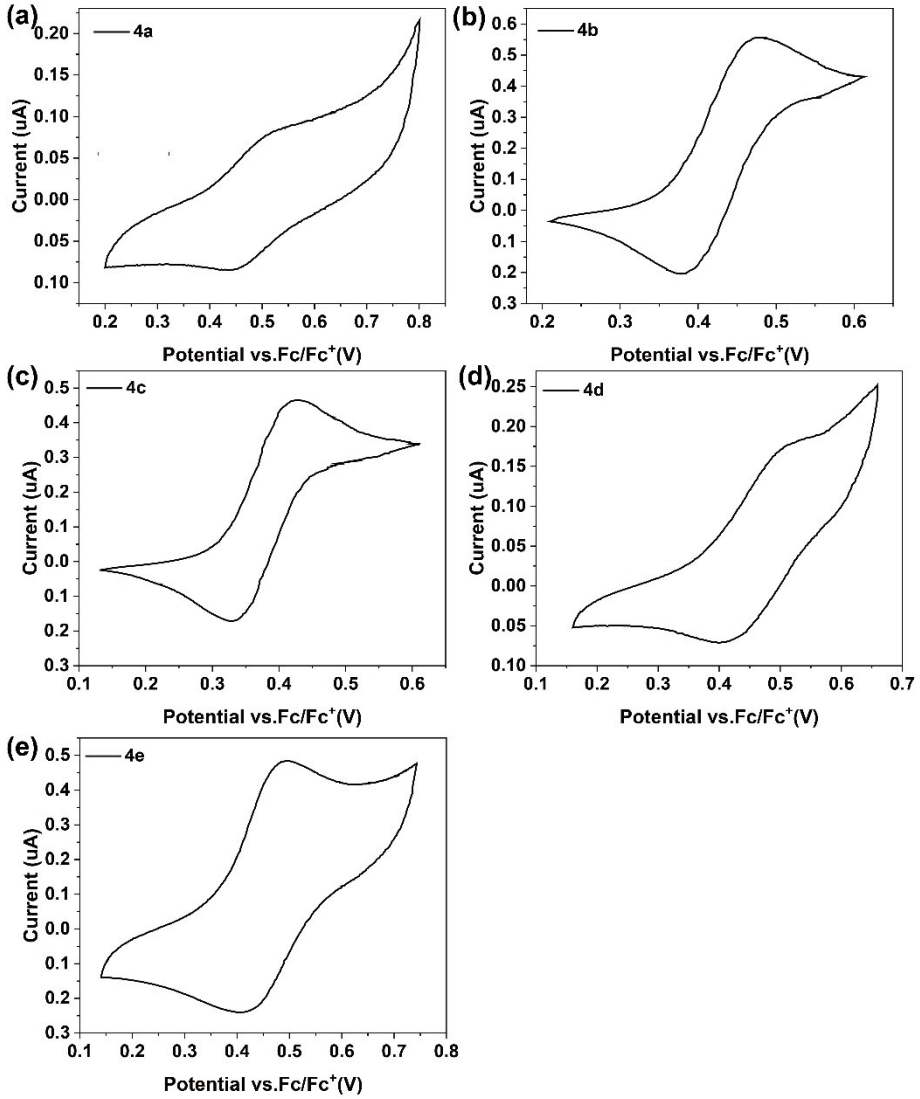

Figure S23. Cyclic voltammograms of **4a**, **4b**, **4c**, **4d**, and **4e** in DCM with $Bu_4N^+BF_6^-$ (0.1 M) as a supporting electrolyte, Fc = ferrocene.

8. Comparison of HOMO/LUMO plots

Table S17 . Electronic properties of **4a**, **4b**, **4c**, **4d**, and **4e**

Entry	E_g[a](eV)	E_{OX}[b](V)	LUMO(eV) (Exp)[c]	HOMO(eV) (Exp)[d]	LUMO(eV) (Cal)[e]	HOMO(eV) (Cal)[e]	E_g(eV) (Cal)[e]
4a	4.84	0.42	-0.38	-5.22	-0.57	-5.65	5.08
4b	3.28	0.37	-1.89	-5.17	-1.85	-5.00	3.16
4c	3.15	0.32	-1.97	-5.12	-1.87	-5.01	3.14
4d	4.18	0.38	-1.00	-5.18	-0.98	-5.44	4.46
4e	3.86	0.36	-1.30	-5.16	-1.27	-5.47	4.20

[a] E_g estimated from the UV-Vis absorption spectra.

[b] Oxidation onset potentials measured by cyclic voltammetry.

[d] HOMO = -(E_{ox} + 4.8) eV.

[c] LUMO = HOMO + E_g.

[e]Theoretical calculations have been carried out by using the GAUSSIAN09 suite of programs in gas-phase at the B3LYP/6-31G(d) levele[7], respectively.

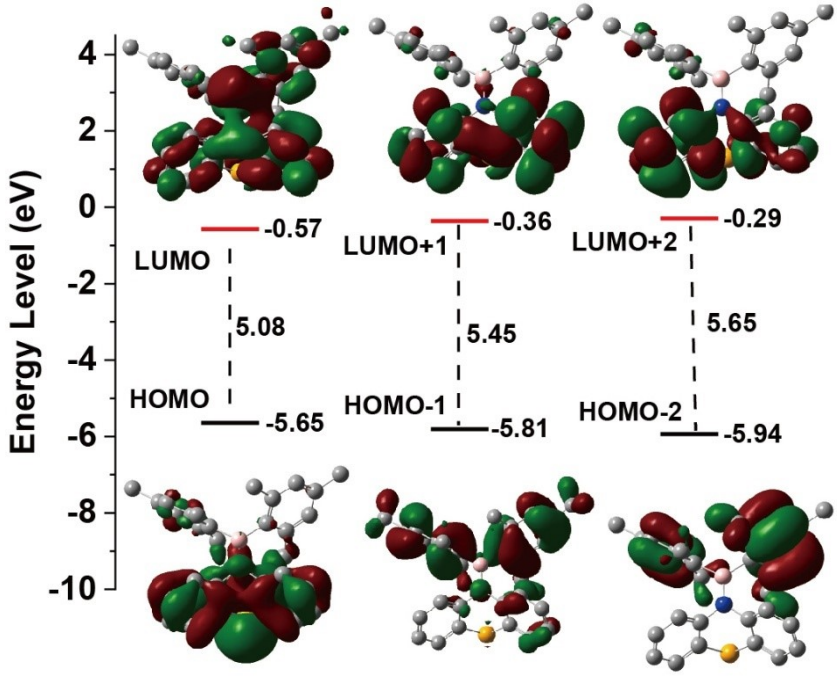

Figure S24. Computed molecular orbital plots for **4a**.

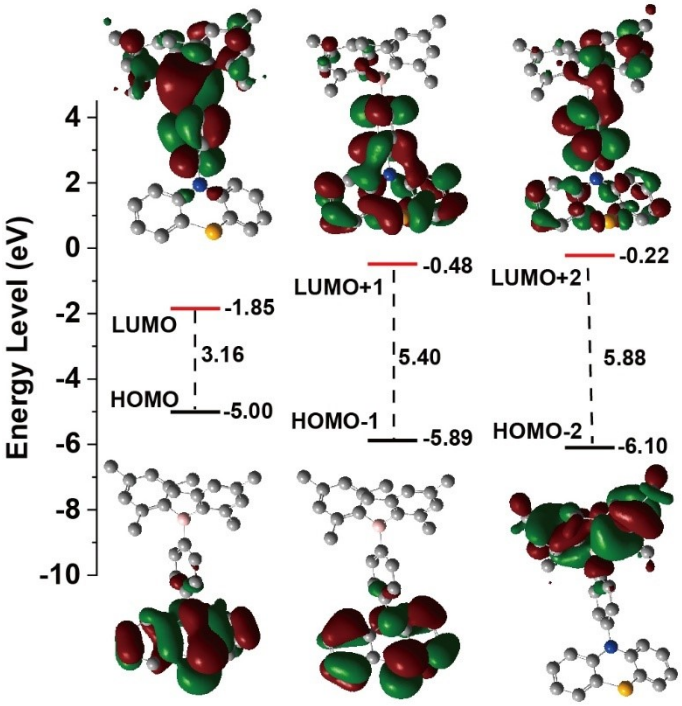

Figure S25. Computed molecular orbital plots for **4b**.

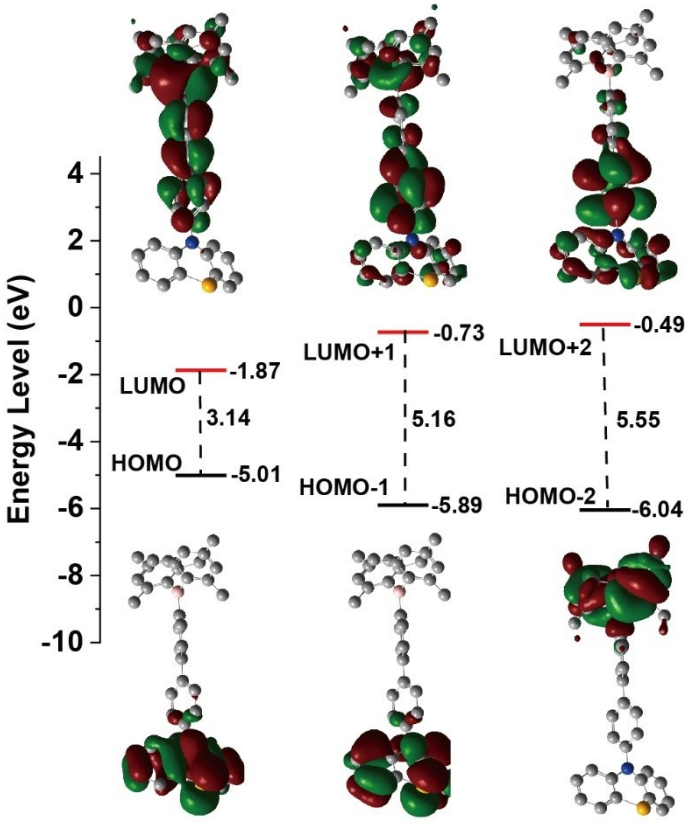

Figure S26. Computed molecular orbital plots for **4c**.

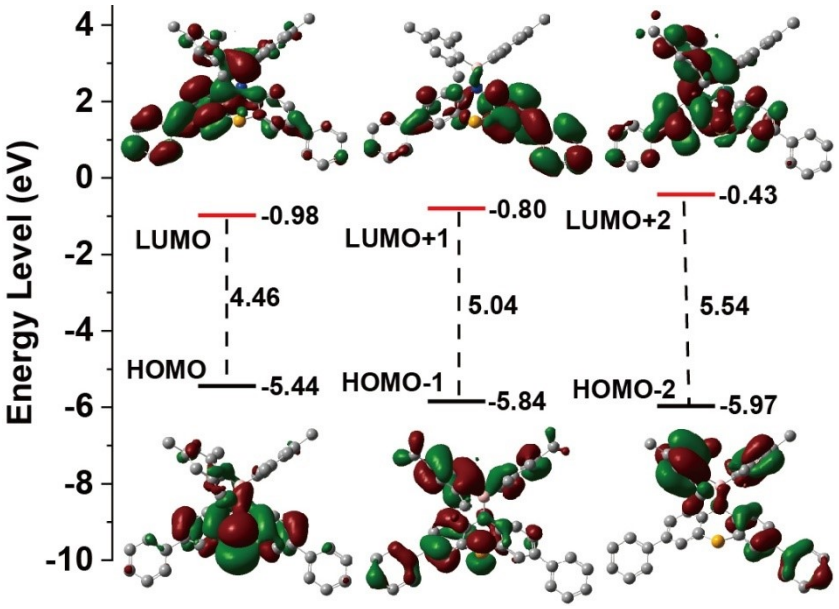

Figure S27. Computed molecular orbital plots for **4d**.

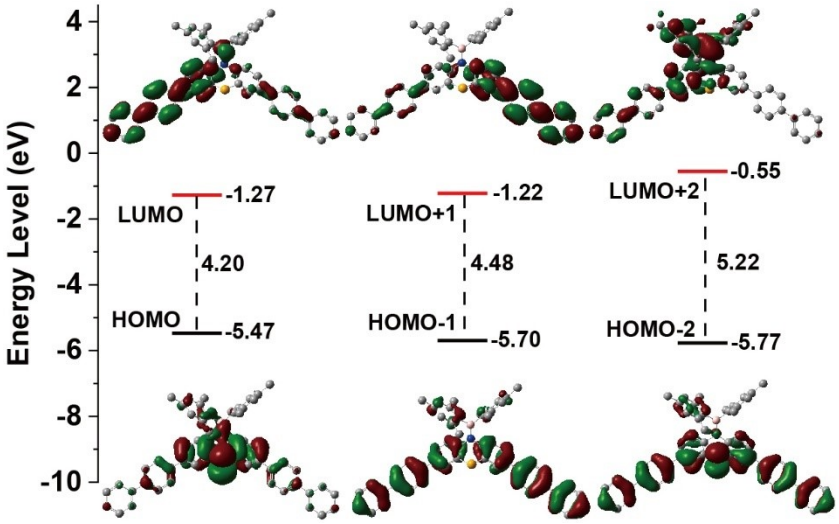

Figure S28. Computed molecular orbital plots for **4e**.

9. Aggregation-induced fluorescence properties

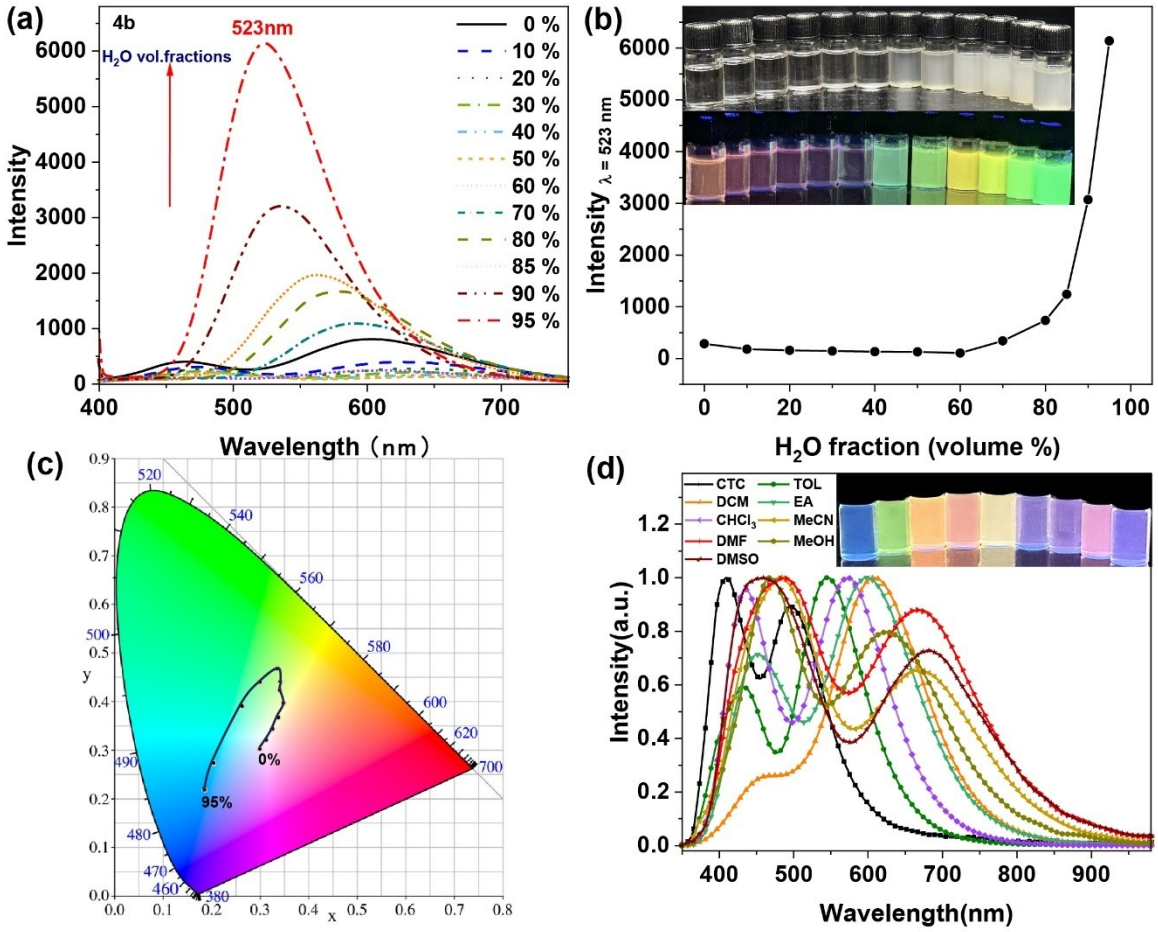

Figure S29. Photoluminescence (PL) spectra of 4b in different THF/water ratios. (a) Photographs of aggregates under UV light, λ_{ex} = 365 nm. (b) Emission intensity of **4b** as the THF/water ratio is altered (fluorescence intensity at 523 nm). (c) CIE chromaticity. (d) Emission spectra of **4b** in solutions (with different polarities).

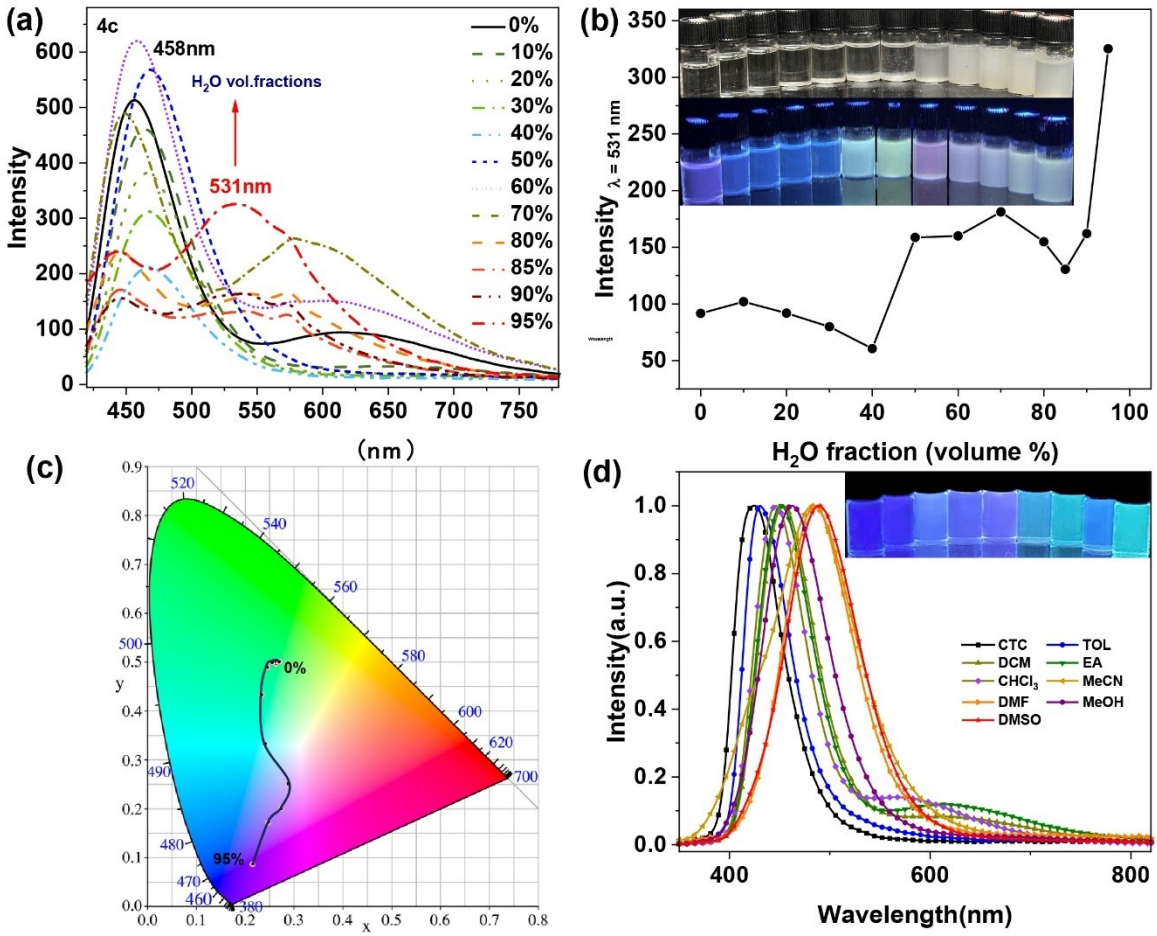

Figure S30. Photoluminescence (PL) spectra of 4b in different THF/water ratios. (a) Photographs of aggregates under UV light, λ_{ex} = 365 nm. (b) Emission intensity of **4c** as the THF/water ratio is altered (fluorescence intensity at 523 nm). (c) CIE chromaticity. (d) Emission spectra of **4c** in solutions (with different polarities).

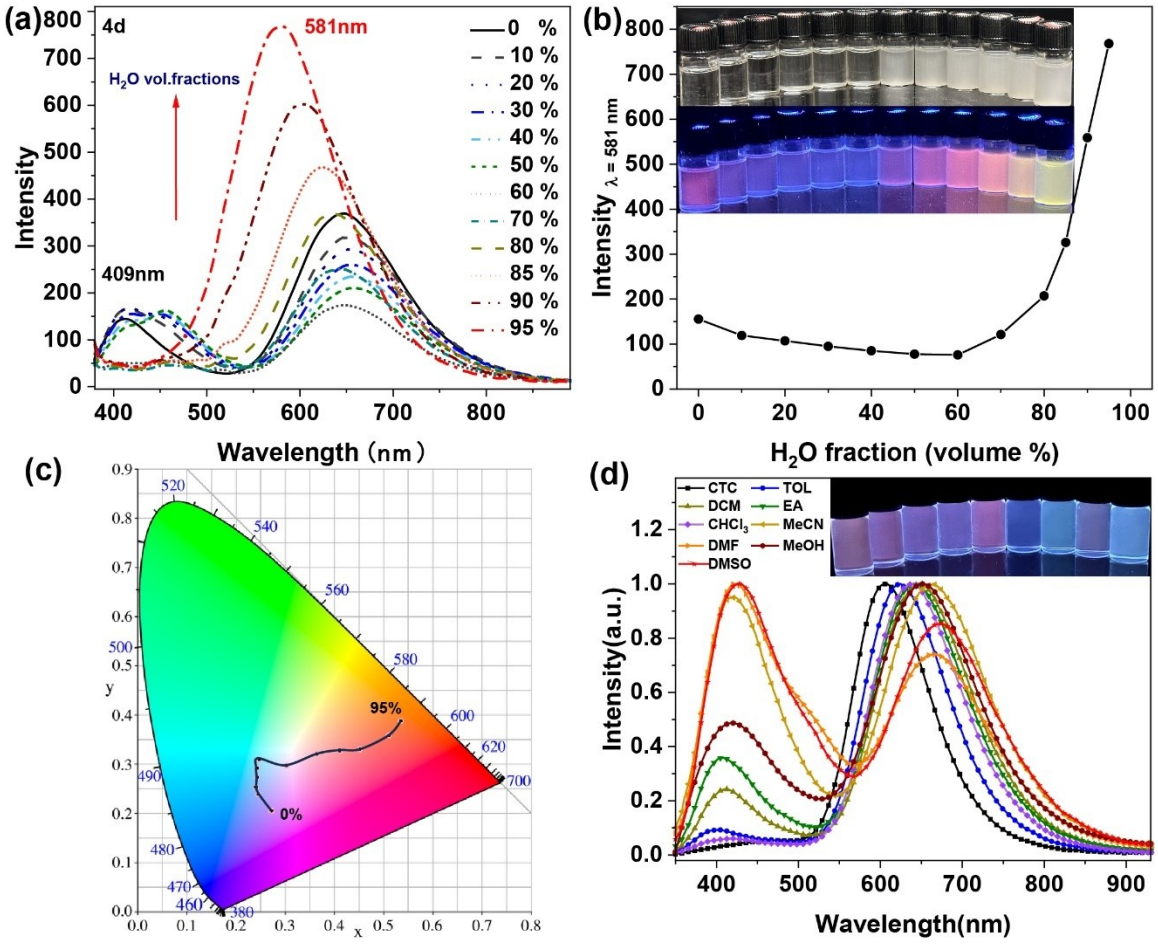

Figure S31. Photoluminescence (PL) spectra of 4b in different THF/water ratios. (a) Photographs of aggregates under UV light, λ_{ex} = 365 nm. (b) Emission intensity of **4d** as the THF/water ratio is altered (fluorescence intensity at 523 nm). (c) CIE chromaticity. (d) Emission spectra of **4d** in solutions (with different polarities).

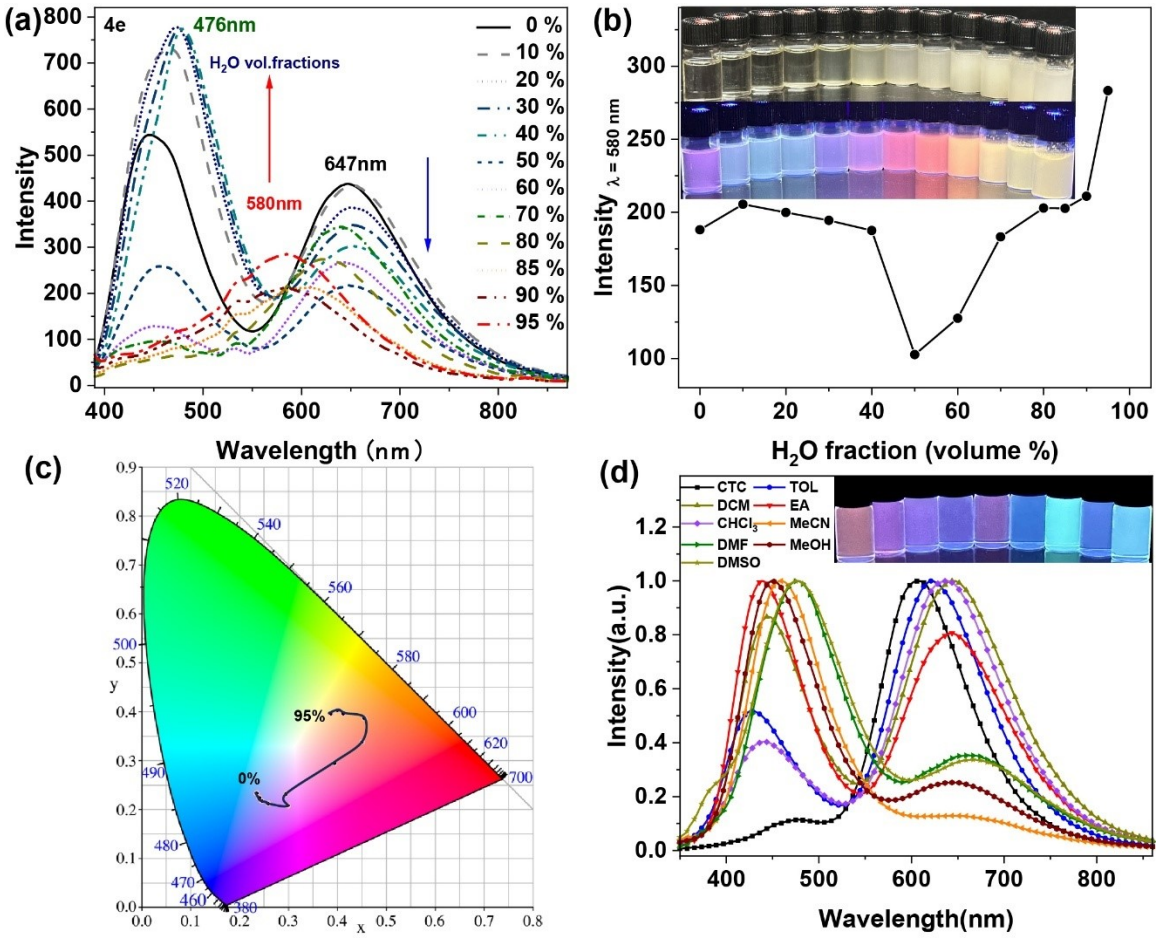

Figure S32. Photoluminescence (PL) spectra of 4b in different THF/water ratios. (a) Photographs of aggregates under UV light, λ_{ex} = 365 nm. (b) Emission intensity of **4e** as the THF/water ratio is altered (fluorescence intensity at 523 nm). (c) CIE chromaticity. (d) Emission spectra of **4e** in solutions (with different polarities).

10. Determination of the detection limit

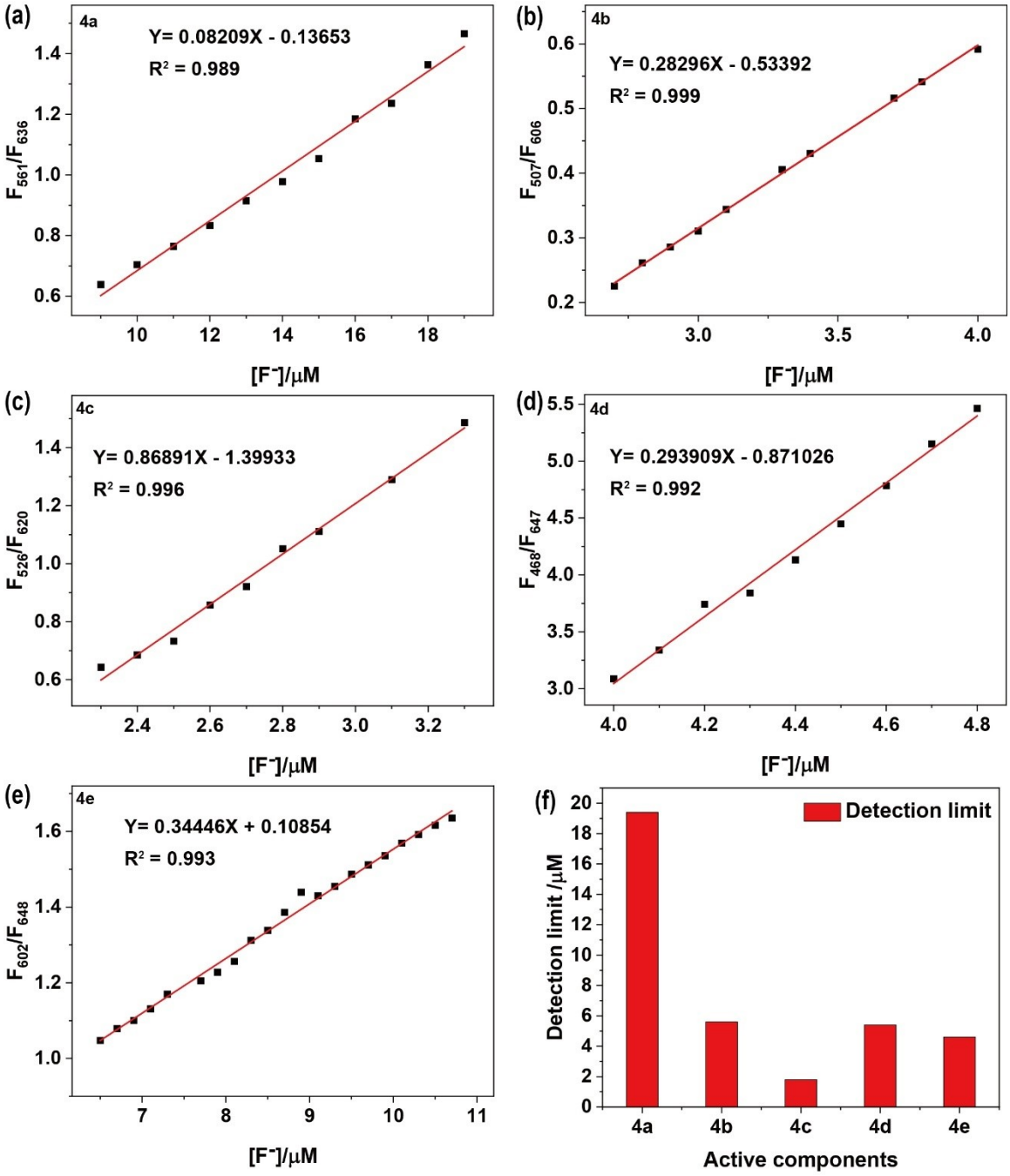

Figure S33. The calibration curves and linear equation for FL intensity and concentration of F^- and the calculated detection limits of **4a**, **4b**, **4c**, **4d**, and **4e**.

11. Electrochromism of 4a in solution and film applied potentials.

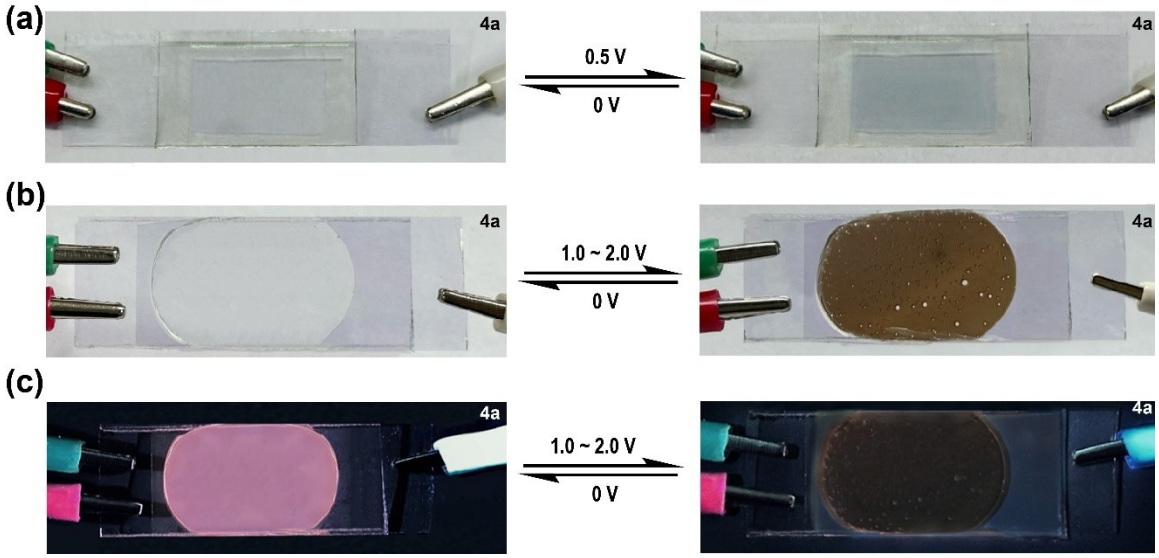

Figure S34. (a) Photos of ECDs with **4a** in DMF solution applied potentials; Photos of ECDs with **4a** in film assemble by polycaprolactone (PCL) applied potentials under daylight lamp (b) and UV illumination (c).

12. optical stability test for electrochromic switching of **4a**, **4d**, and **4e**.

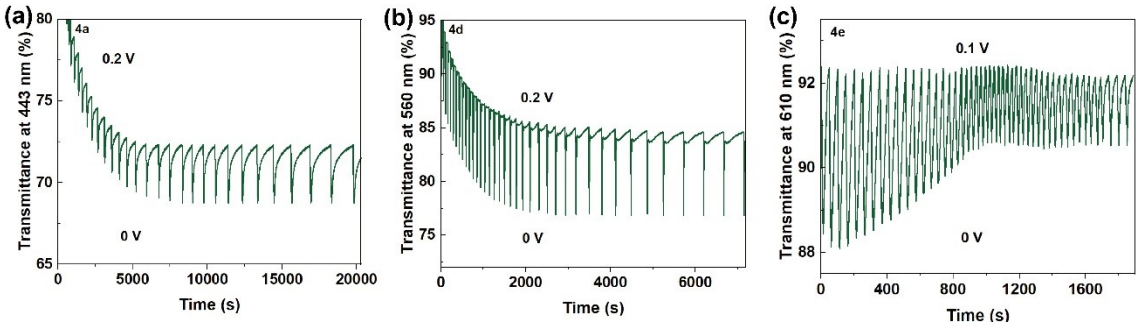

Figure S35. Optical stability test for electrochromic switching of **4a, 4c**, and **4d**

13. Fluorescence spectral changes of **4a**, **4d**, and **4e** film applied potentials.

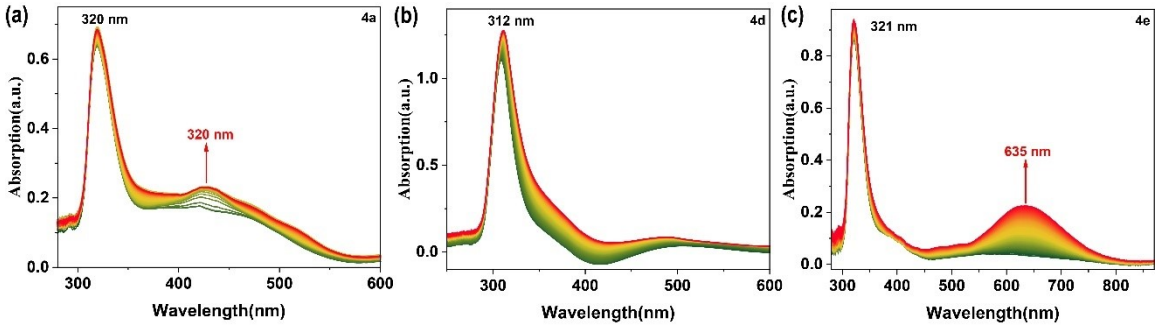

Figure S36. The UV/vis absorption spectral changes of **4a**, **4d**, and **4e** applied potentials in the film.

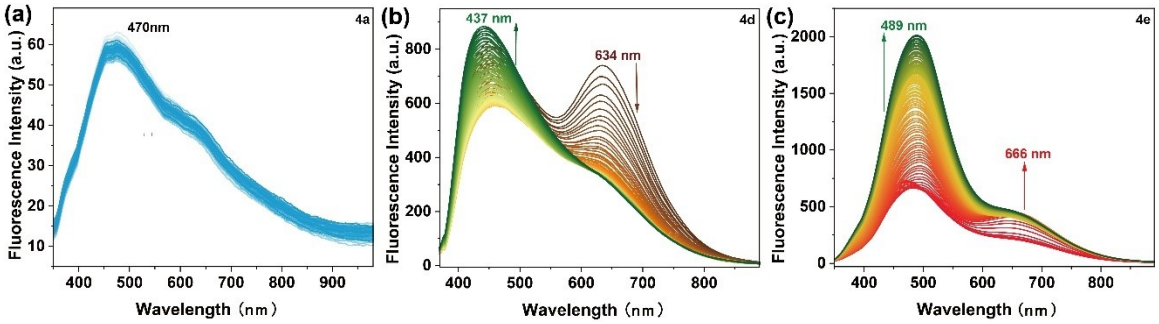

Figure S37. Fluorescence spectral changes of **4a**, **4d**, and **4e** applied potentials in the film.

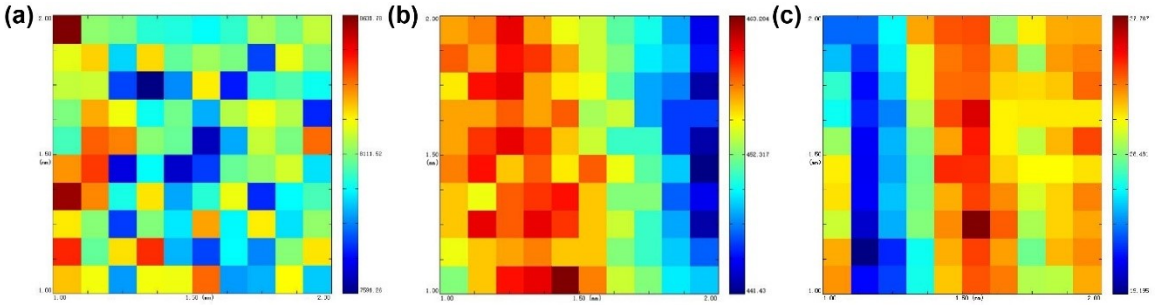

Figure S38. The two-dimensional diagram of **4a**, **4d**, and **4e** in the film.

.

14. ^{1}H NMR and ^{13}C NMR spectra

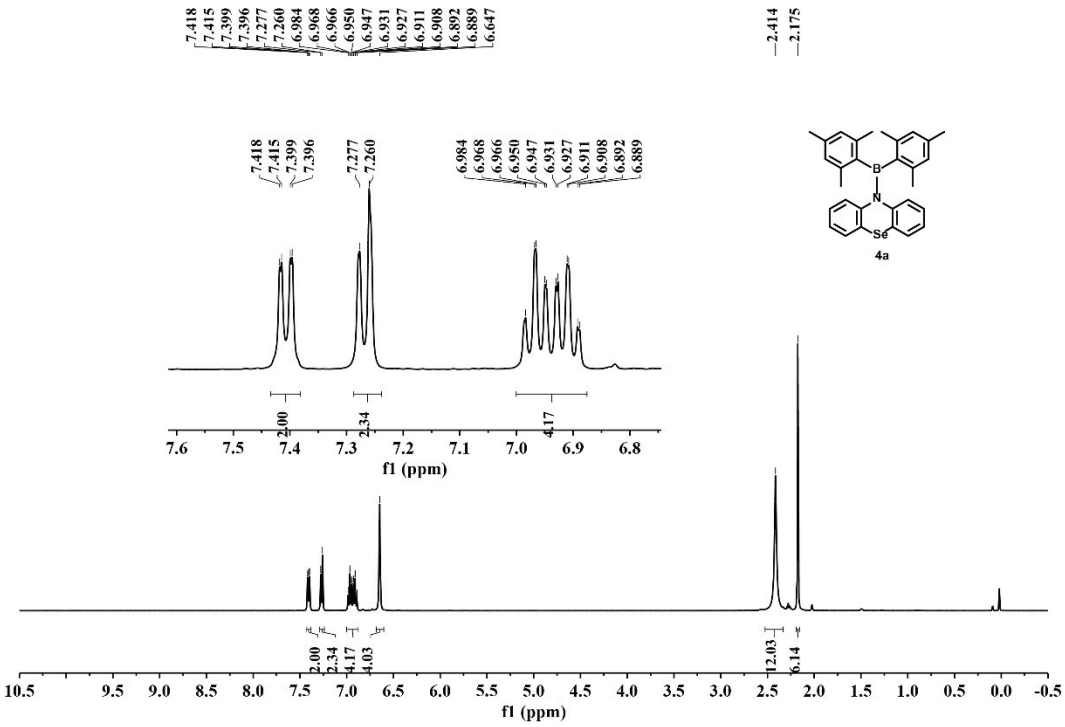

^{1}H NMR spectrum of **4a** in $CDCl_3$

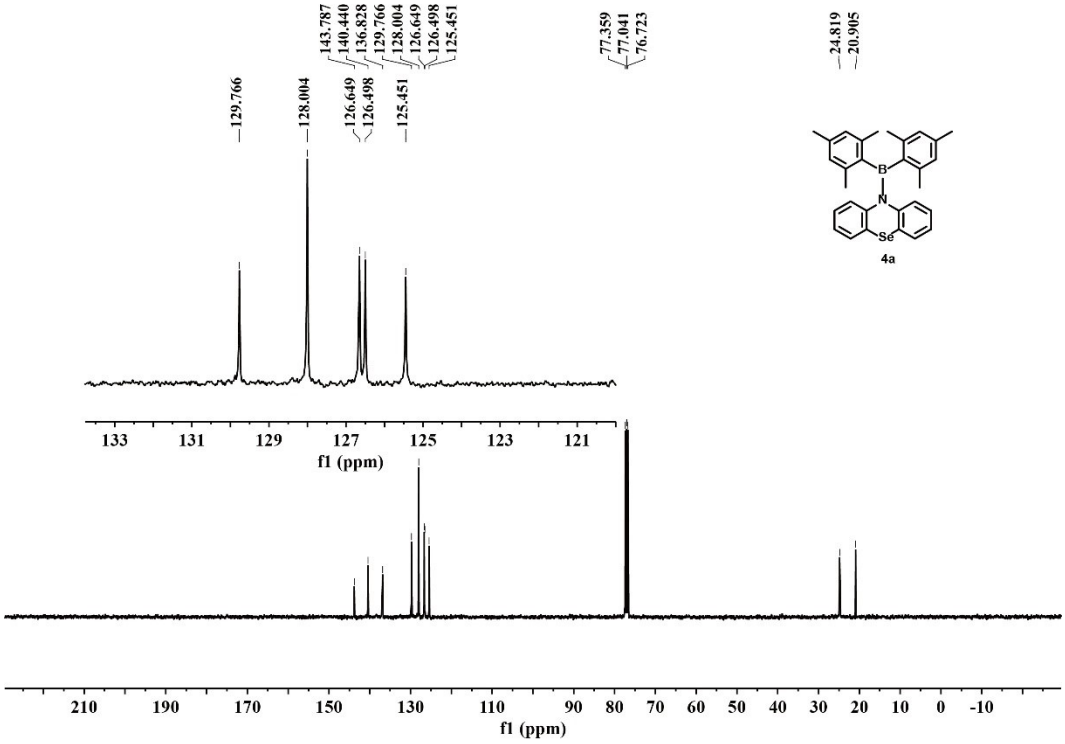

^{13}C NMR spectrum of **4a** in $CDCl_3$

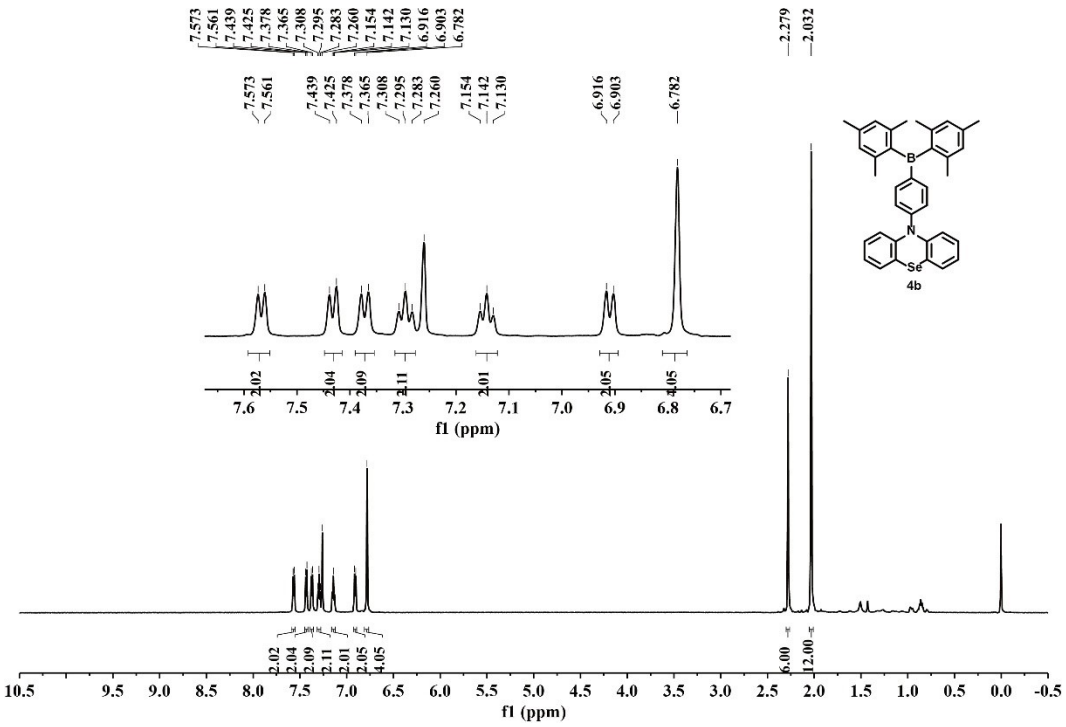

^{1}H NMR spectrum of **4b** in $CDCl_3$

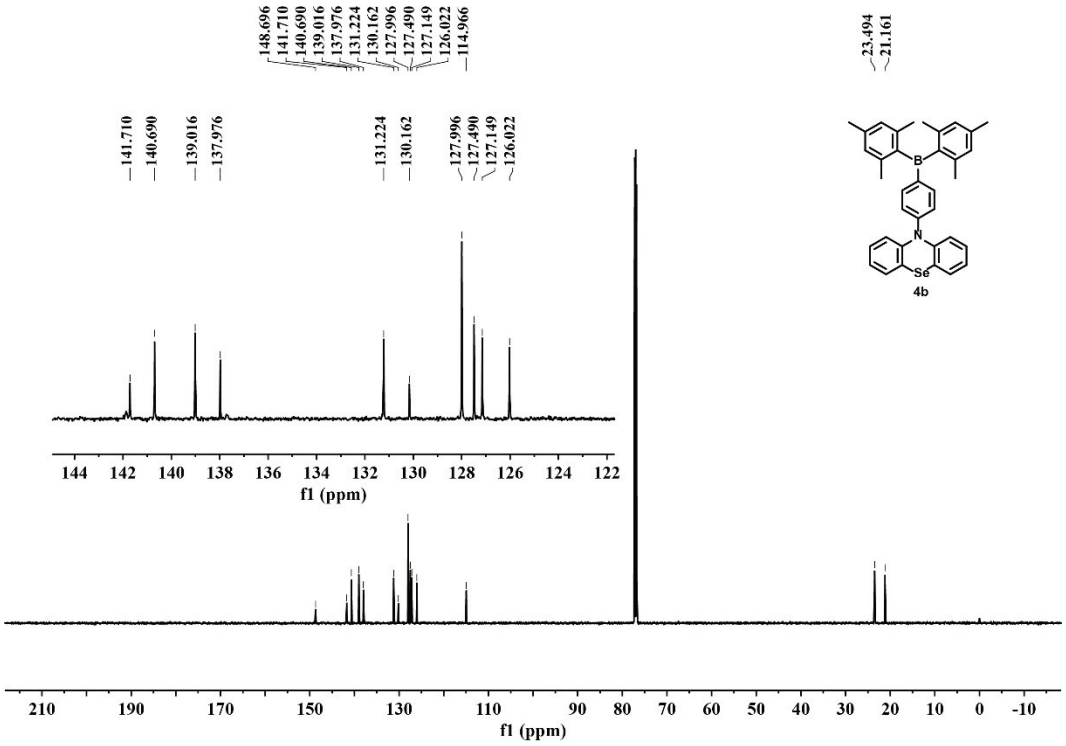

^{13}C NMR spectrum of **4b** in $CDCl_3$

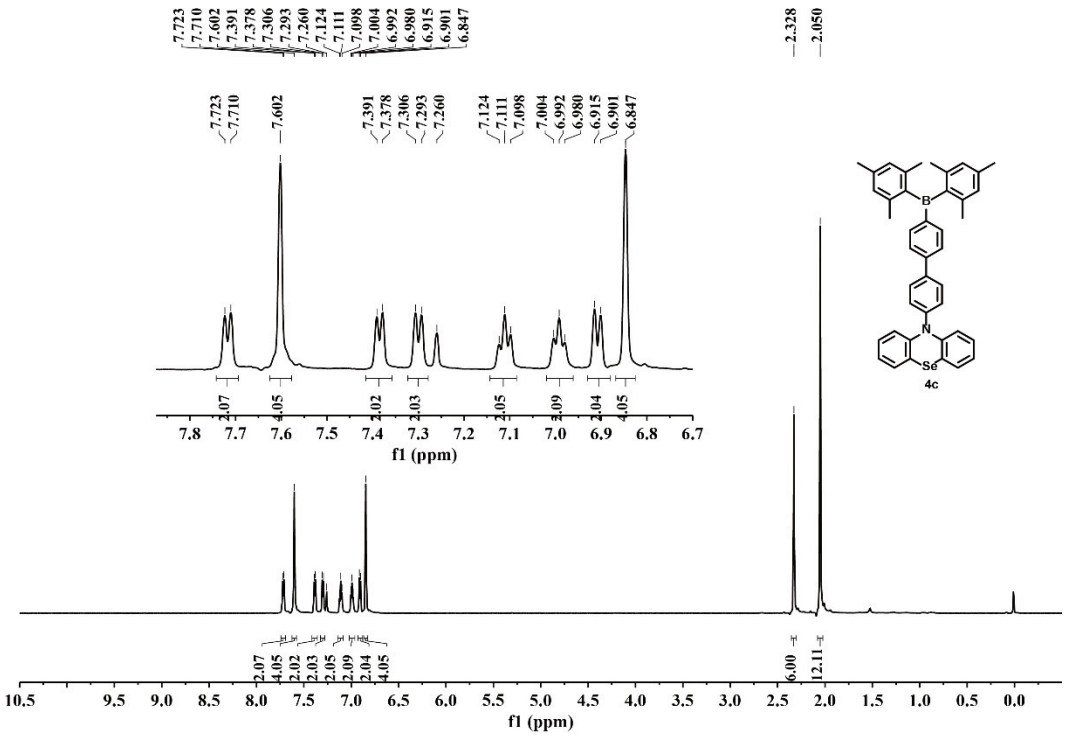

^{1}H NMR spectrum of **4c** in $CDCl_3$

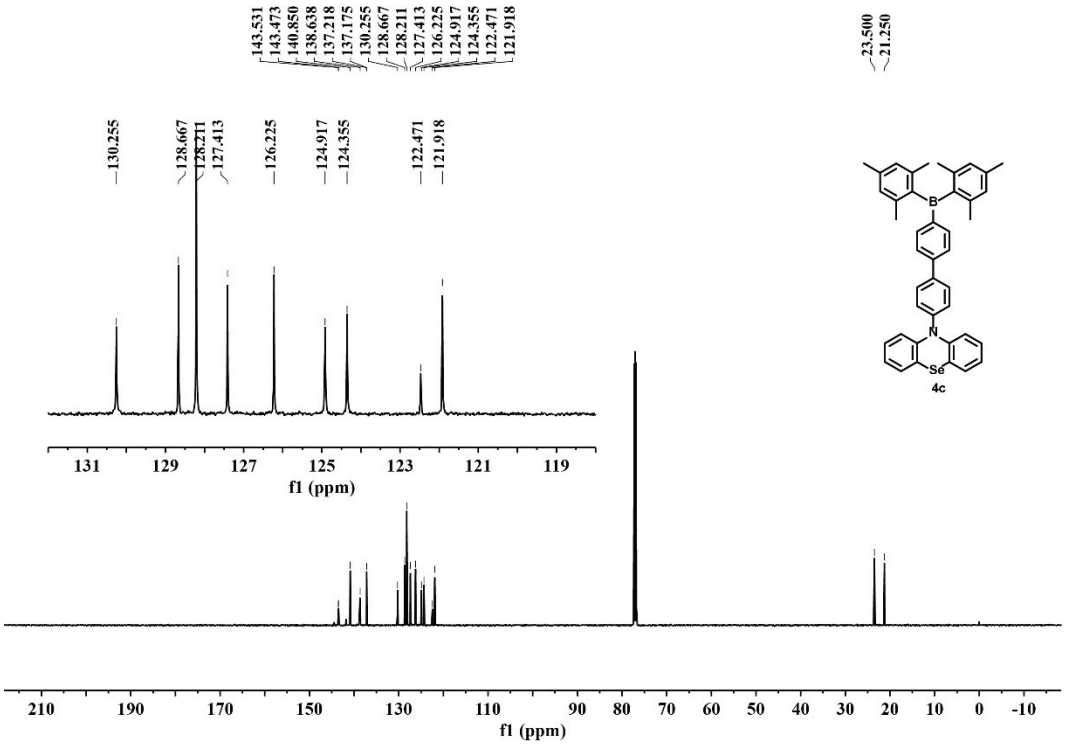

^{13}C NMR spectrum of **4c** in $CDCl_3$

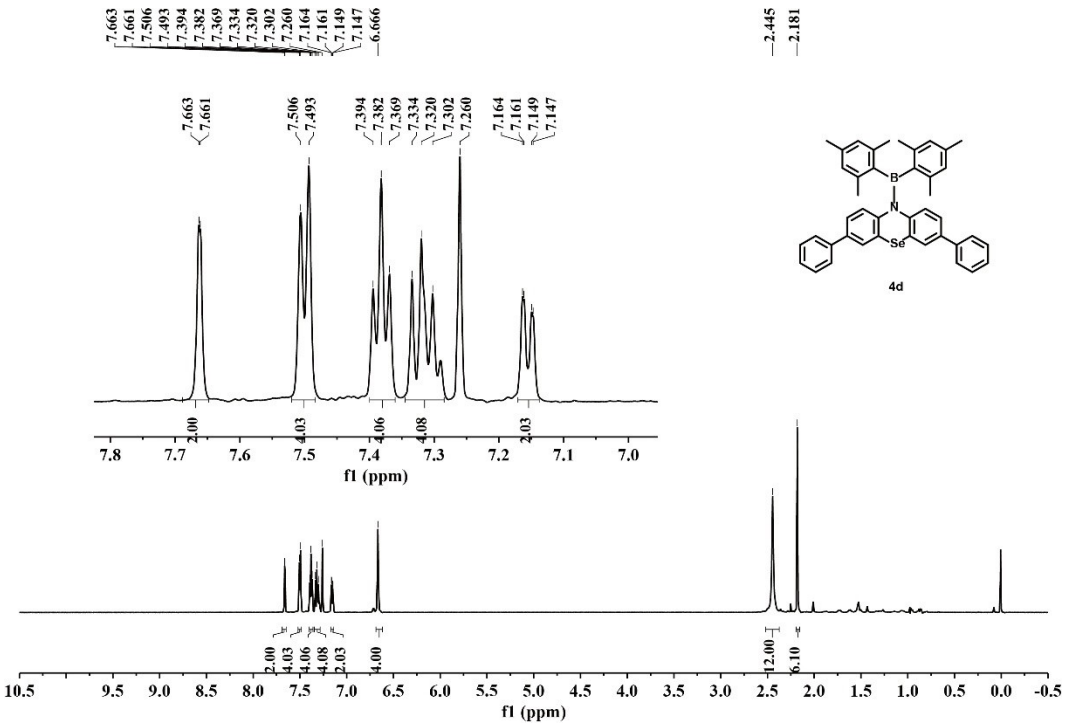

^{1}H NMR spectrum of **4d** in $CDCl_3$

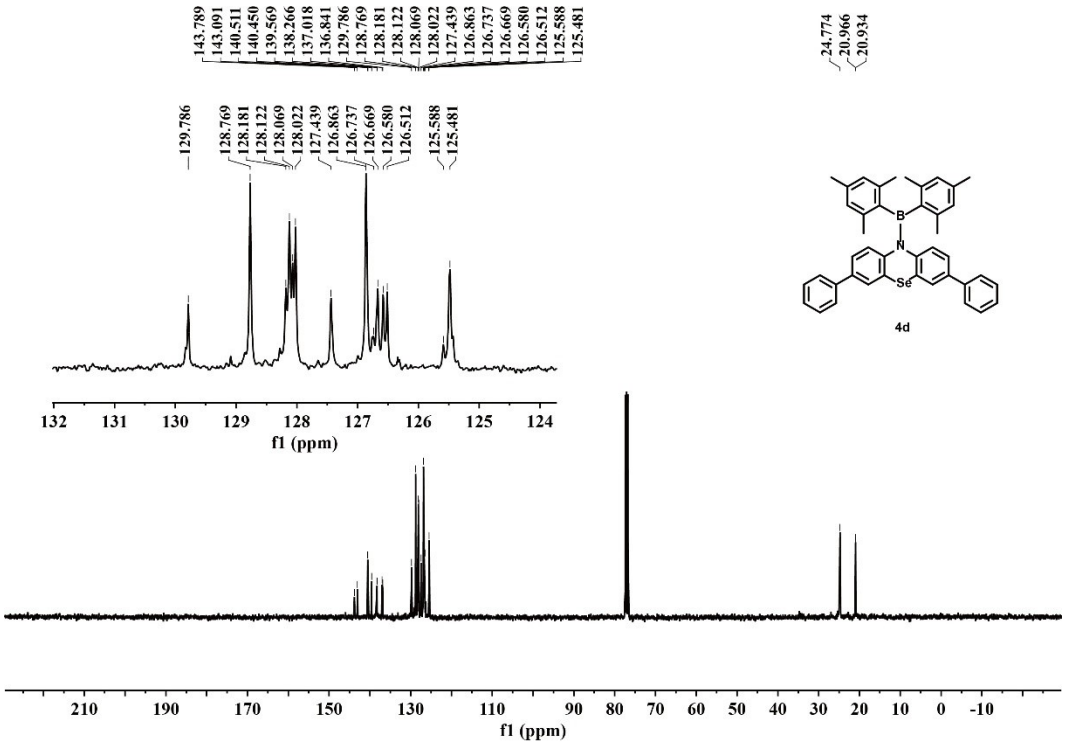

^{13}C NMR spectrum of **4d** in $CDCl_3$

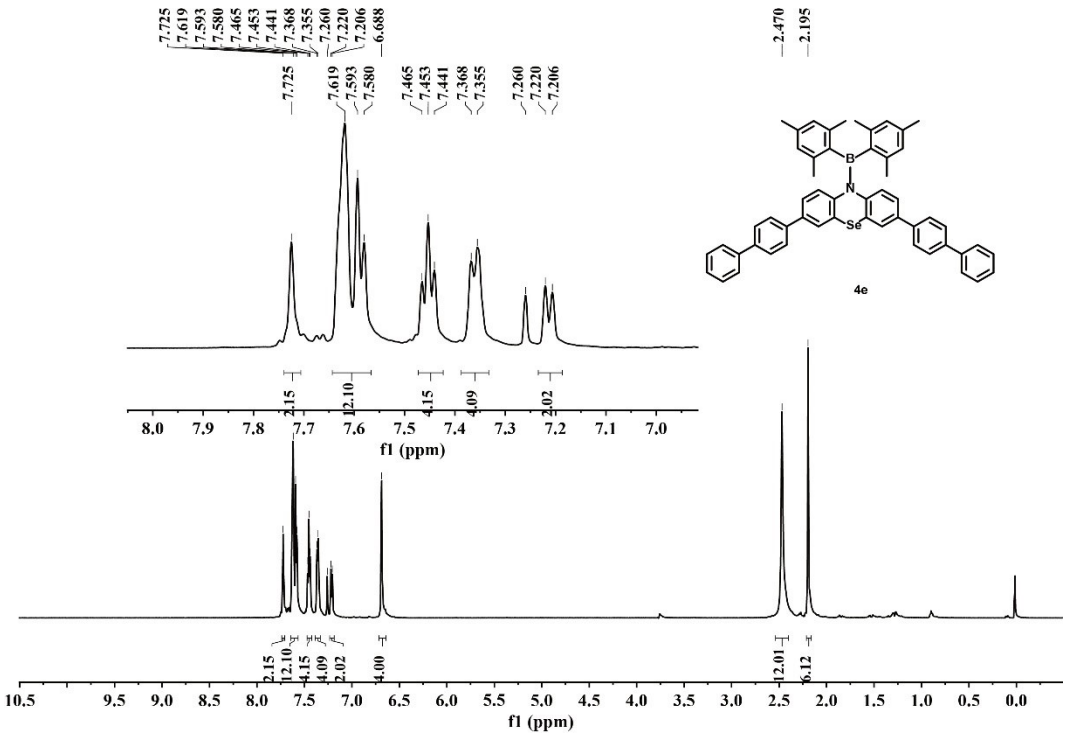

^{1}H NMR spectrum of **4e** in $CDCl_3$

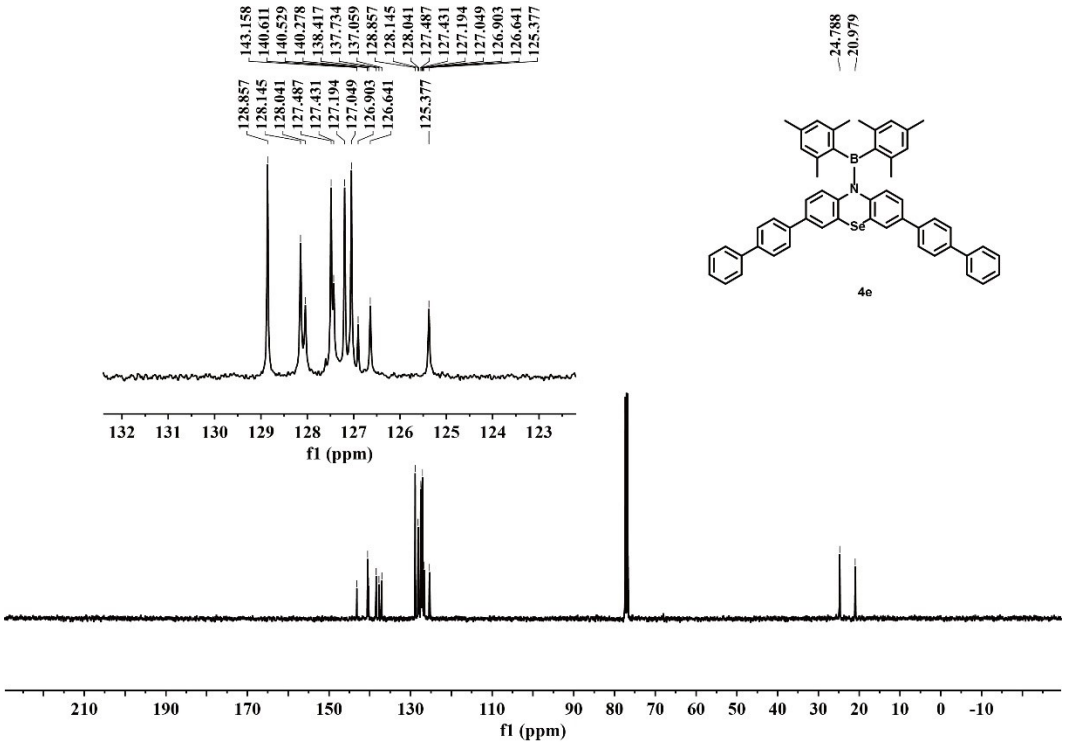

^{13}C NMR spectrum of **4e** in $CDCl_3$

15. HRMS spectra

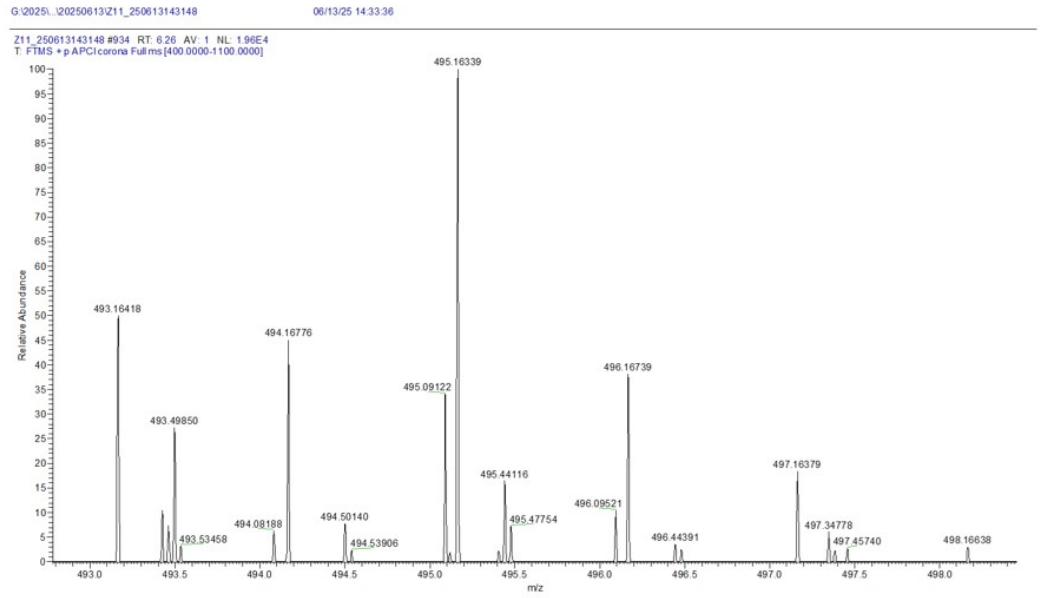

HRMS of **4a**

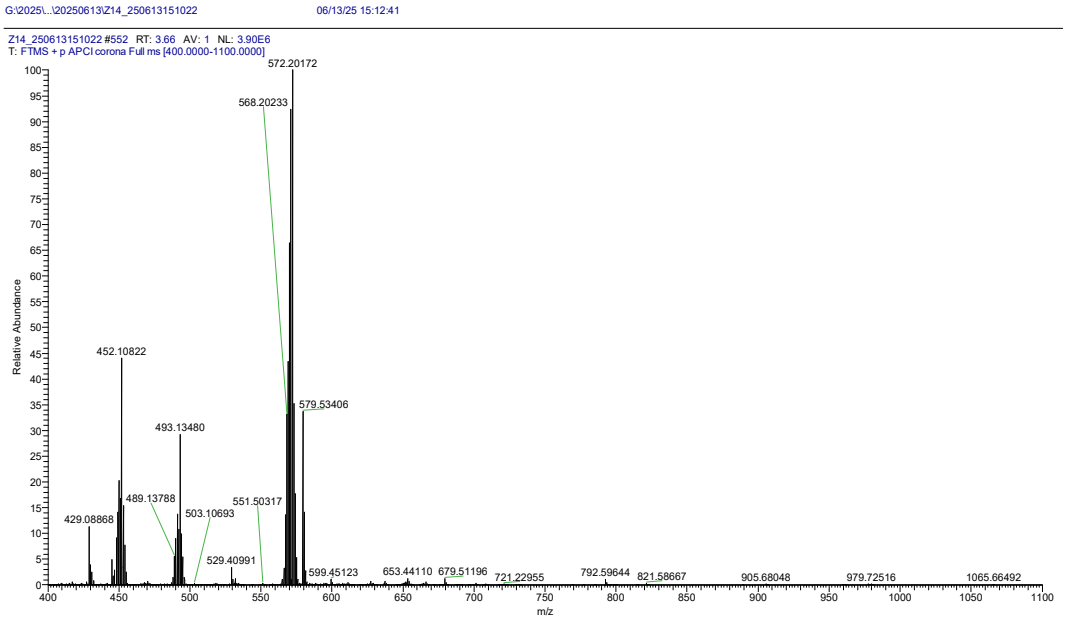

HRMS of **4b**

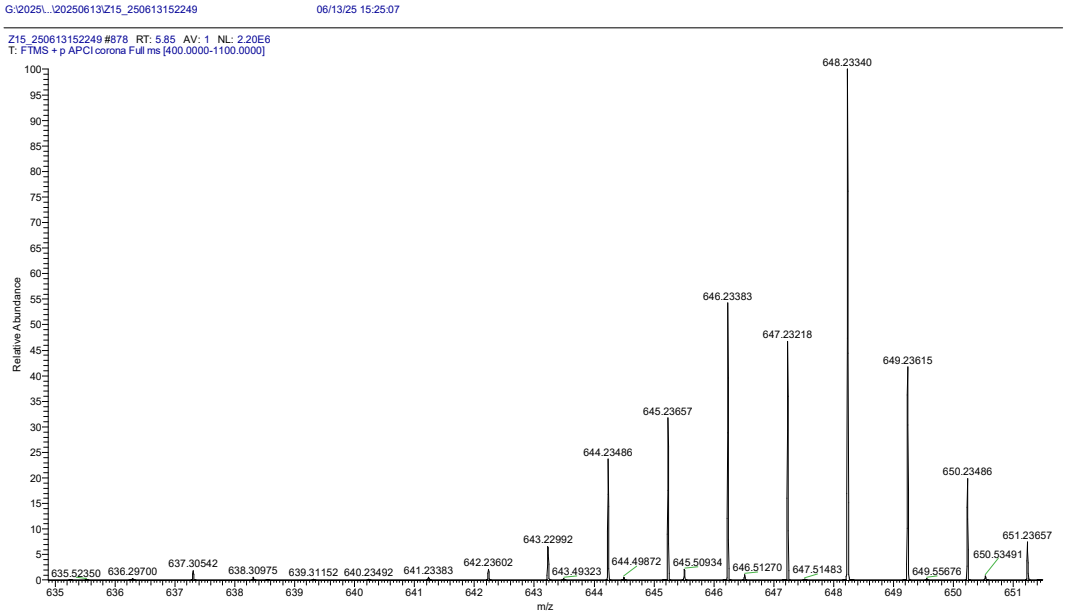

HRMS of **4c**

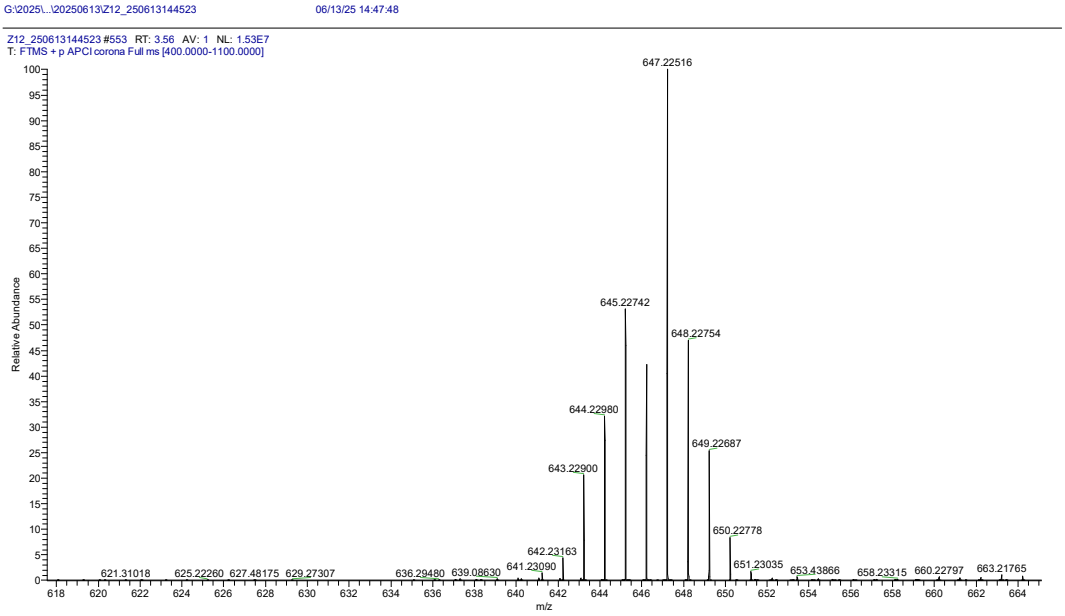

HRMS of **4d**

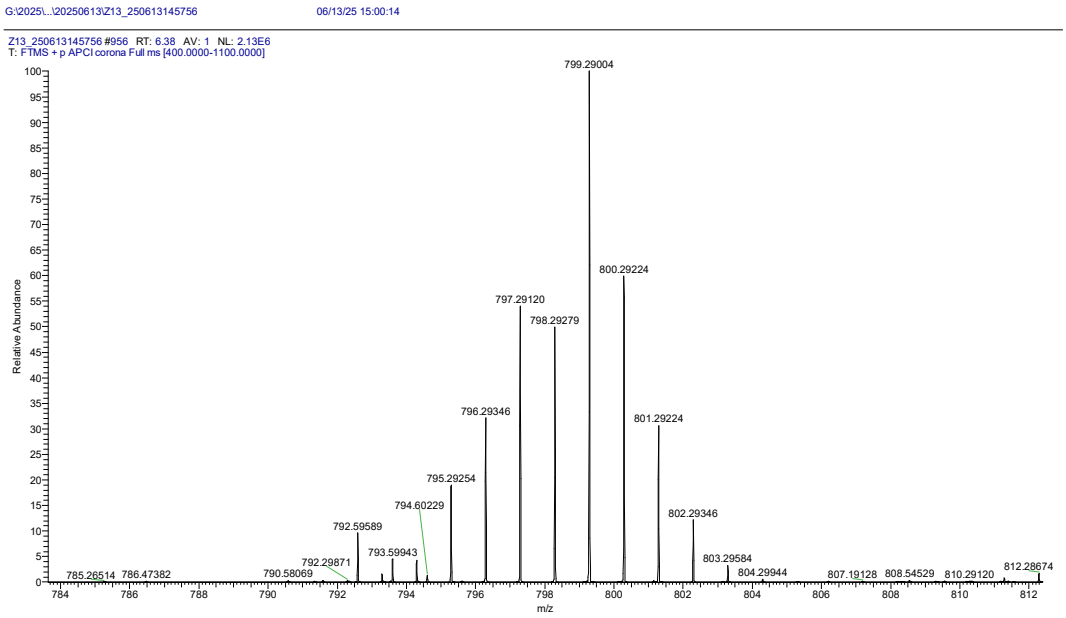

HRMS of **4e**

16. Reference

[1] X. Cao, K. Pan, J. Miao, X. Lv, Z. Huang, F. Ni, X. Yin, Y. Wei, C. Yang, *J. Am. Chem. Soc.*, 2022, **144**, 22976-22984.

[2] Z. Zhang, B. Zhang, X. Han, H. Chen, C. Xue, M. Peng, G. Ma, Y. Ren, *Chem. Sci.*, 2023, **14**, 2990-2998.

[3] C. J. Cramer, D. G. Truhlar, *Chem. Rev.*, 1999, **99**, 2161-2200.

[4] R. Cammi, J. Tomasi, *J. Comput. Chem.*, 1995, **16**, 1449-1458.

[5] J. Tomasi, M. Persico, *Chem. Rev.*, 1994, **94**, 2027-2094.

[6] S. Miertuš, E. Scrocco, J. Tomasi, *Chem. Phys.*, 1981, **55**, 117-129.

[7] M. Frisch, *Inc, Wallingford CT.* 2009, **201**.